Empirical mode decomposition based algorithm for islanding detection in micro-grids

Electric Power Systems Research 201 (2021) 107542

Contents lists available at ScienceDirect

Electric Power Systems Research

journal homepage: www.elsevier.com/locate/epsr

Empirical mode decomposition based algorithm for islanding detection in micro-grids

Hasan Khosravi [a], Haidar Samet [a,b,*], Mohsen Tajdinian [a]

[a] Department of Power and Control Engineering, School of Electrical and Computer Engineering, Shiraz University, Shiraz, Iran
[b] Department of Electrical Engineering, Eindhoven University of Technology, Eindhoven, the Netherlands

ARTICLE INFO

Keywords:
Renewable energy resources
Islanding
Distributed generation
Empirical mode decomposition

ABSTRACT

Owning to extensively enhancement of renewable energy resources in the distribution grids, the employment of such sources is also associated with various issues such as the islanding problem. In this paper, an effective method has been proposed for detection of the islanding in the micro-grids comprised of inverter or direct fed types of distributed generations. The proposed method is designed based on the intrinsic modes of the voltage signal measured at the PCC point. More specifically, through the calculation of the positive sequence of the voltage signal variation (PSVSV) and extracting the signal energy of PSVSV's intrinsic modes, the islanding can be detected. The superiority of the proposed islanding detection method is manifested in the condition where the generation of distributed resources is in balance with the loading consumption. The performance of the proposed method has been evaluated considering the conditions where islanding is difficult to detect or might be mistaken with other phenomena given by loads within the NDZ region, different fault types, and loads with different power factors. The performance evaluation has been carried out through simulations, and furthermore has been compared with the state-of-the-art algorithms.

1. Introduction

With the increasing demand for electrical energy, the growing concerns upon the environmental and geographical issues of the fossil fuel -based energy sources, distributed generation (DG) has been growingly raised a lot of popularity amongst the power industry technicians, and investors. The distributed generation is generally considered as the generation of electricity at the place of consumption. However, such a term is mostly referred to the renewable energy sources presently. On account of the high costs of power transmission, and distribution, the DG-based power can be accessed more economically. Many countries have targeted for a great share of renewable energy-based electricity generation. In the USA and Europe, DG has developed into a technologically- and financially- feasible solution. Several methods have been proposed in [1] for the utilization of DGs with a few to ten kilowatts.

The importance of protecting DGs from islanding is indicated where DGs are parallelly in operation with distribution systems. The islanding phenomenon is referred to as the condition where a power system is subjected to an operational interruption while the DGs continue to generate. The voltages and the frequency of the islanded section cannot be controlled through the operation of DGs. Moreover, an islanded condition is associated with power quality degradation and hazardous life risks to the utility personnel. Given the adversities of unintentional islanded conditions, being introduced upon the growth of DG installments [2], the detection of such a phenomenon is of high importance.

Several standards have been introduced regarding the islanding phenomenon, such as UL 1741, IEEE 1547, and IEEE 929 [3]. Moreover, different islanding detection methods have been proposed over the years. These methods, classified into two main groups of remote and local -control approaches, have been tabulated in Table 1. The remote control -based methods operate based on the connection of the DG and the main network. Although these methods demonstrate a reasonable performance, they are not economically affordable. One of these remote methods is based on the supervisory control and data acquisition (SCADA) system, which constantly analyzes every possibility for islanding conditions [4, 5]. The utilization of power transmission lines for connection of DGs and the main network is yet another remote controlling method [6, 7]. The main idea behind the local control methods is the regional monitoring of system parameters such as voltage, frequency, etc.

The local control methods are grouped into three main categories,

* Corresponding author.
E-mail address: samet@shirazu.ac.ir (H. Samet).

https://doi.org/10.1016/j.epsr.2021.107542
Received 4 December 2020; Received in revised form 4 May 2021; Accepted 20 August 2021
Available online 3 September 2021

Table 1
Various islanding detection methods.

Islanding detection technique		Advantages	Disadvantages	Example
Remote control		* High accuracy	* Very high costs, especially in small networks	- Power line signaling
		* Reliable		- Transfer Trip Method
Local control	Passive Approaches	* Low detection time		- over/under voltage and over/under frequency
		* No disturbances applied to the system	* Big NDZ region	- rate of change of frequency (ROCOF)
		* High accuracy in case of unbalance between generation and consumption	* Complicated threshold defining	- phase jump detection (PJD)
				- voltage harmonics distortion
				- rate of change of frequency over power (ROCOFOP)
				- voltage unbalance
				- rate of change of sequence components of current
				- inverse hyperbolic secant function (IHSF)
				-rate of change of voltage phase angle
				- rate of change of frequency (ROCOF)
				- phase jump detection (PJD)
	Active Approaches	* Small NDZ region		
			* Disturbance injection to the system	- Active ROCOF
			* Degraded power quality	- sliding mode frequency shift (SMFS)
			* Low detection speed due to time interval required for system response analysis	- current injection
			* Application of disturbances by specific time margins when	- active and reactive power control loops for synchronous
				mostly being unnecessary
				* Degraded power quality
	Hybrid Approaches	* Small NDZ region	* Application of both passive and active methods together, resulting in high detection time	- combination of rate of change of reactive power (ROCOQ) with load connecting
			* Application of disturbances only when required	- combination of ROCOV (where V stands for voltage) with real power shift
				- voltage fluctuation injection scheme that combined ROCOF or ROCOV with correlation factor (CF) methods
				- optimized sandia frequency shift (SFS) and ROCOF
				- combination of ROCOV (where V stands for voltage) with real power shift

given by passive, active, and hybrid approaches. The passive methods operated based on the measurement of specific system parameters. However, in case of low inequality between the load consumption, and the DG power, the system parameters do not represent such a notable variation to detect the islanding condition from. Therefore, the decision making solely based on the parameter variations is not rather reliable. Some of the passive methods are given as Over/Under voltage and Over/Under frequency, rate of change of frequency (ROCOF), phase jump detection (PJD), voltage harmonics distortion, rate of change of frequency over power (ROCOFOP), voltage unbalance, rate of change of sequence components of current, inverse hyperbolic secant function (IHSF) and rate of change of voltage phase angle [8–11]. The deficiencies of the passive methods, even in the case of load and generation balance, are solved through the application of active approaches. These methods act upon the injection of a small disturbance to the system for islanding detection. Even a small disturbance can cause a big variation in an islanded system, which can be used for islanding detection, with respect to the insignificant variations occurred in an interconnected system. Such methods defect considering disturbance injection, power quality degradation, and low detection speed due to the time interval required for analyzing the system's response to the applied disturbance. Additionally, the disturbance, being applied to the system at specific time intervals, is mostly unnecessary. Some of the most important active islanding detection approaches are given as: active ROCOF [12], sliding mode frequency shift (SMFS) [13], current injection [14,15], active and

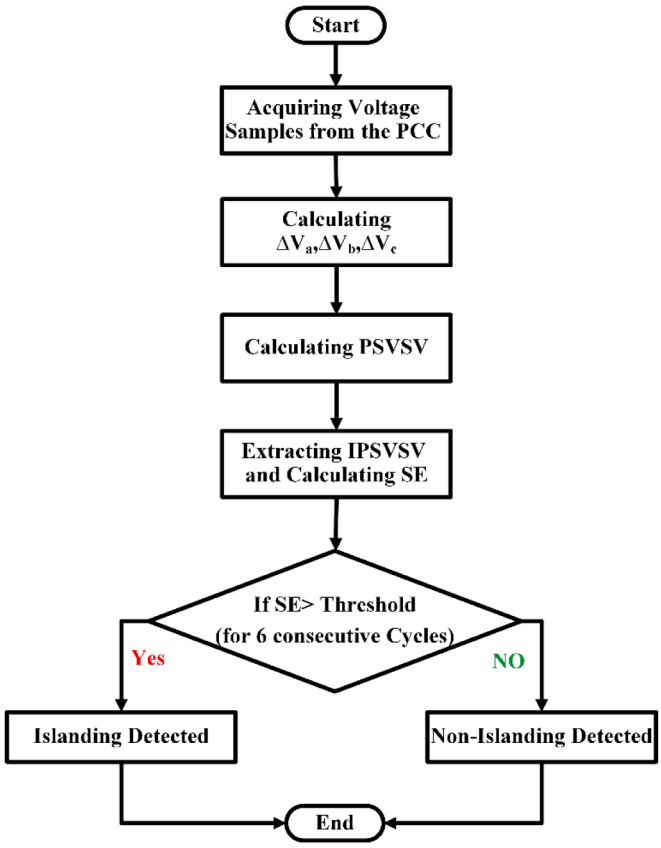

Fig. 1. Procedure of proposed method implementation.

reactive power control loops for synchronous distributed generator [16]. The islanding condition can be detected with the use of hybrid methods, combining the passive and active methods, thus benefiting from the capabilities of both methods. Some of the typical hybrid methods are given as combination of Rate of Change of Reactive Power (ROCOQ) with Load Connecting Strategy, combination of ROCOV (where V stands for voltage) with Real Power Shift, Voltage Fluctuation Injection scheme that combined ROCOF or ROCOV with Correlation Factor (CF) methods, optimized Sandia Frequency Shift (SFS) and ROCOF [17,18].

Recently, several passive anti-islanding algorithms based on the time-frequency analysis including wavelet transform (WT) and S-transform have been addressed in the publications [19–24]. By employing PCC voltage and current signals, these transforms are utilized to extract information regarding signal's energy or high frequency components. In essence, WT cannot be considered as a real time-frequency analysis and it generally provides a time-scale analysis with non-adaptive nature. Non-adaptive nature means the selected the mother wavelet cannot be changed during the analysis and it must be utilized to analyze all the data. Besides, in the WT analysis, simultaneous same accuracy for a time or frequency dependent information cannot be expected. Combining the short time Fourier transform (STFT) and the wavelet transform, S-transform is known as one of the powerful time-frequency analysis which can be employed to perform multi-resolution analysis and to extract the frequency information. Comparing to other time-frequency based methods, S-transform has more time consuming. Hilbert–Huang Transform (HHT) is another powerful tool for time-frequency analysis of stationary and non- stationary signals that is proposed for islanding detection [25–27]. HHT which is established on the empirical mode decomposition (EMD), has an adaptive nature to extract feature of signals. The advantages of HHT over S-transform and WT have been reported in [28,29]. Several algorithms signal decomposition techniques based on the EMD [30–33], transient monitoring function (TMF) [34,35], mathematical morphology (MM) [36], and matrix pencil (MP) [37], variational mode decomposition (VMD) [38] and ensemble EMD [39], have been reported for islanding detection purposes. In [37], it has been reported that matrix pencil (MP) suffers from the selecting threshold corresponding to singular value. Note that the applications of signal decomposition techniques including ensemble EMD and empirical wavelet transform (EWT) in power system studies have been reported in [40,41]. In general, time-frequency methods suffer from vulnerability against noisy conditions and require high-sampling rate.

Generally, it can be deduced that the most important deficiency of the passive methods is their inability of islanding detection in the case of balance between DG power and load consumption. Even though such an issue is tackled by active methods; nevertheless, due to a constantly applied disturbance to the system, the power quality is degraded and, thus, such methods are not commonly popular. In hybrid methods, the disturbances are only applied to the system when being required, and therefore such methods are more noted.

In this paper, a novel approach has been proposed for the detection of islanding condition considering the different types of DGs. To such end, the voltage signal is measured at the PCC point, and thereafter, the instantaneous positive sequence of the voltage signal variation (PSVSV) are extracted. Afterward, EMD is employed to extract first intrinsic mode functions (IMF) of PSVSV. Finally, an index is proposed that calculates the signal energy of first IMF of PSVSV. As it will be demonstrated, the proposed index can clearly differ for islanded and non-islanded conditions after a short time interval. One of the advantages of this method is its ability to perform under the condition of balance between generation and consumption (the NDZ region can be ignored). In addition, unlike active approaches [12–16], the proposed method does not affect the normal operation of the network and its power quality. Moreover, unlike the previous EMD based approaches which calculate frequency dependent parameters [32], the proposed method is based on the PSVSV. PSVSV can be easily obtained from voltage signals obtained from instrument transformer and as a result, the proposed method does not require any further frequency estimation processes.

This paper constitutes of the following sections: in Section 2, the islanding detection algorithm in micro-grids is presented. The

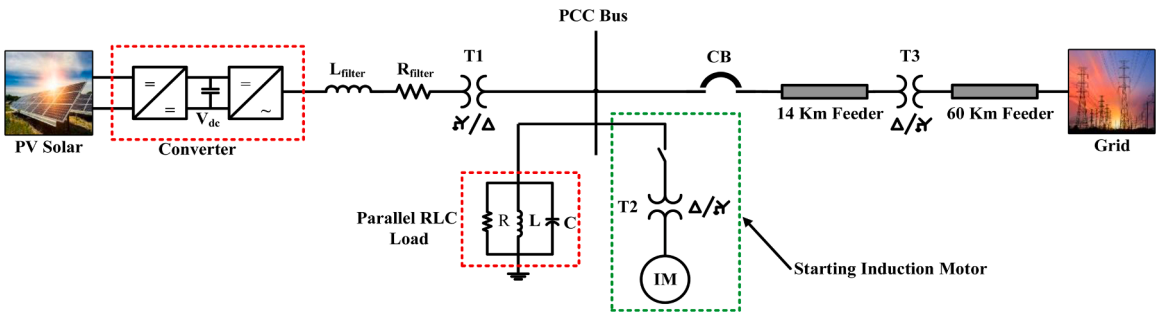

Fig. 2. Test system for performance evaluation.

Table 2
Microgrid specification.

Component	Value
PV Panel	
Output Power	240 kW
PWM Carrier Frequency	1980 Hz
Input DC voltage	480 V
PV Output Voltage (Line to Line)	250 V
Transformer T1	
Nominal Power	500 KVA
Resistance of winding 1 &2	0.0012 p.u.
Inductance of winding 1 &2	0.03 p.u.
Magnetization Resistance	200 Ω
Magnetization Inductance	200 Ω
Winding 1 Voltage (Line to Line)	250 V
Winding 2 (Grid Side) Voltage (Line to Line)	$16\sqrt{3}$ kV
Transformer T2	
Nominal Power	2.5 MVA
Resistance of winding 1 & 2	0.0015 p.u.
Inductance of winding 1&2	0.035 p.u.
Magnetization Resistance	250 Ω
Magnetization Inductance	250 Ω
Winding 1 Voltage (Line to Line)	400 V
Winding 2 Voltage (Line to Line)	$16\sqrt{3}$ kV
Transformer T3	
Nominal Power	47 MVA
Resistance of winding 1 & 2	0.00267 p.u.
Inductance of winding 1 & 2	0.08 p.u.
Magnetization Resistance	200 Ω
Magnetization Inductance	200 Ω
Winding 1 Voltage (Line to Line)	132 kV
Winding 2 Voltage (Line to Line)	$16\sqrt{3}$ kV
RLC Load	
$R_{Local\ load}$	3.2 kΩ
$L_{Local\ load}$	8.49 H
$C_{Local\ load}$	0.829 μF
Load Quality Factor	1
Load Resonant Frequency	60 Hz
Nominal Grid Frequency	60 Hz
Induction Motor	
Power	10 - 100KVA
Voltag	400 V
Stator Resistance (R_s)	0.0425 p.u.
Stator Inductance (L_s)	0.087 p.u.
Rotor Resistance (R_r)	0.05 p.u.
Rotor Inductance (L_r)	0.0658 p.u.
Mutual Inductance (L_m)	2.9745 p.u.
Inertia Constant	0.09526 p.u.
Pole pairs	2

simulation results are provided in Section 3. Hardware validation and performance comparison are provided in Sections 4 and 5. Finally, conclusion is provided in Section 6.

2. Proposed islanding detection algorithm

2.1. Empirical mode decomposition

As mentioned in [42], EMD is an algorithm that decomposes the signal into several components so-called intrinsic mode function (IMF). IMF's of a signal is identified when the following conditions are satisfied:

- The number of zero-crossings and extrema points becomes the same (or at most varying by one).
- At each point, the mean value of the upper and lower envelopes of the signal becomes zero.

In summary, the procedure of extracting IMFs through EMD can be implemented as follows:

Step (1): Having signal, $x(t)$, all of the local extrema of the signal is determined.

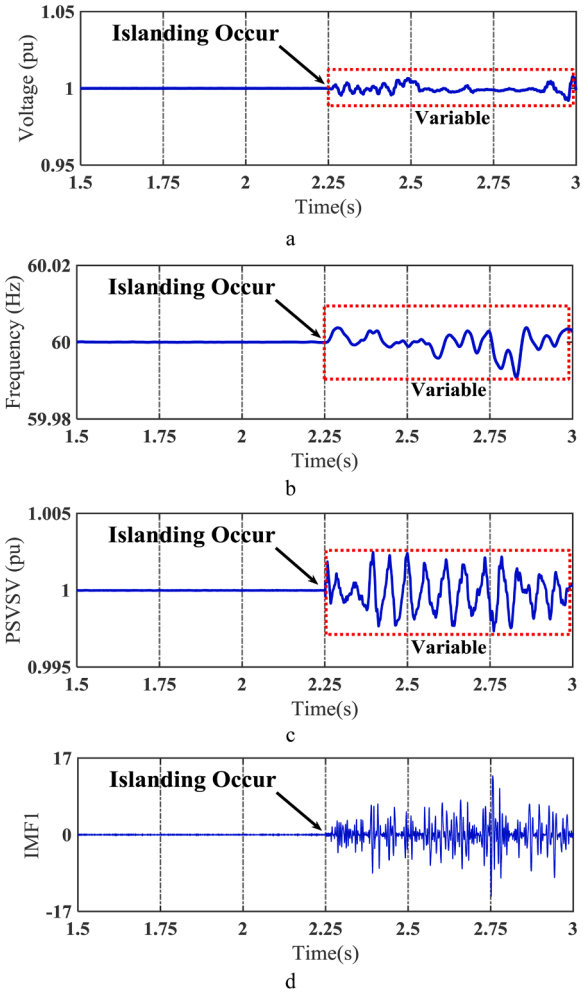

Fig. 3. Sample case for illustration of islanding (a) voltage magnitude, (b) frequency, (c) PSVSV, (d) first IMF.

Table 3
Different type of islanding and non - islanding.

No.	Type of disturbance			No. of events
1	Islanding	ΔP	-50% to +50%	100
		ΔQ	-5% to +5%	
2	Faults	LLLG	$R_f = 0.05 - 30\Omega$	15
		LLL	$R_f = 0.05 - 30\Omega$	15
		LLG	$R_f = 0.05 - 30\Omega$	15
		LL	$R_f = 0.05 - 30\Omega$	15
		LG	$R_f = 0.05 - 30\Omega$	15
3	Load switching	1 – 10 MVA		10
4	Capacitor bank switching	0.1 -1MVAR		10
5	Motor Starting	10 – 100 KVA		10
6	sudden change of load pf	0.7 lag – unit PF		7

Step (2): Knowing local extrema, all of the identified signal's maxima are connected with natural cubic spline lines to find the upper envelope, $u(t)$. Same procedure is performed for the identified signal's minima to find the lower envelope, $l(t)$.

Step (3): Calculating the mean of the upper and lower envelopes as follows:

$$m(t) = [u(t) + l(t)]/2 \quad (1)$$

Step (4): Calculating the difference between the signal, $x(t)$, and the mean of the envelopes, $m(t)$, as follows:

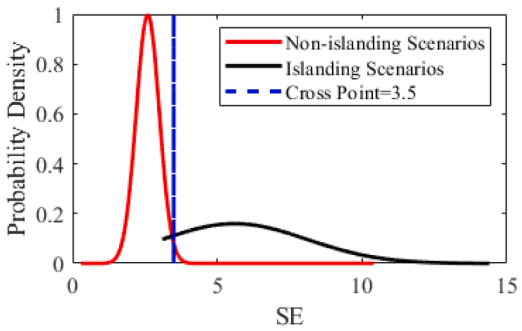

Fig. 4. PDFs for the SE index in the first cycle and the selected threshold in two bus test system (i.e. test system in Fig. 2).

Table 4
Load parameter for UL 1741 testing.

No of Cases	Active Power [%]	Reactive Power [%]	R [kΩ]	L [H]	C [μF]
1	100	100	3.2	8.49	0.829
2	110	100	2.91	8.49	0.829
3	100	99	3.2	8.576	0.829

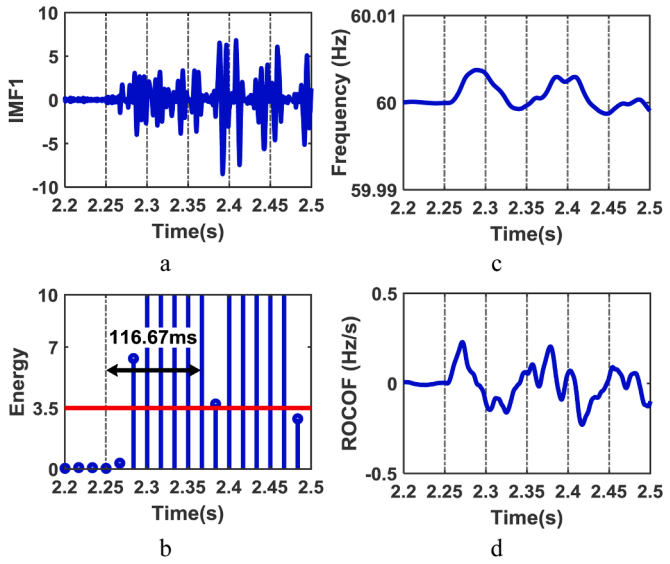

Fig. 5. Performance evaluation under UL 1741 standard, Case 1 (a) first IMF, (b) signal energy of first IMF, (c) frequency, (d) ROCOF.

$$h(t) = x(t) - m(t) \tag{2}$$

Step (5): Checking, $h(t)$, whether if it is satisfied IMF's definition. At this stage, and to avoid increasing the repetition of the IMF screening process, a stoppage criterion is determined which is defined as follows:

$$SD = \sum_{t=0}^{T} \left[\frac{|h_{1(k-1)}(t) - h_{1k}(t)|^2}{h^2_{1(k-1)}(t)} \right] \tag{3}$$

where, SD denotes standard deviation and it varies between 0.2 to 0.3.

Step (6) If, $h(t)$, cannot satisfy the IMF's definition, the steps 1 to 5 on $h(t)$ so that the IMF's definition for certain, $h(t)$, is satisfied.

Step (7) Once, $h(t)$, satisfy the IMF's definition, $h(t)$, is selected as an IMF component, $c(t)$.

Step (8) Calculating the residue of the original signal and the IMF can be done as follows:

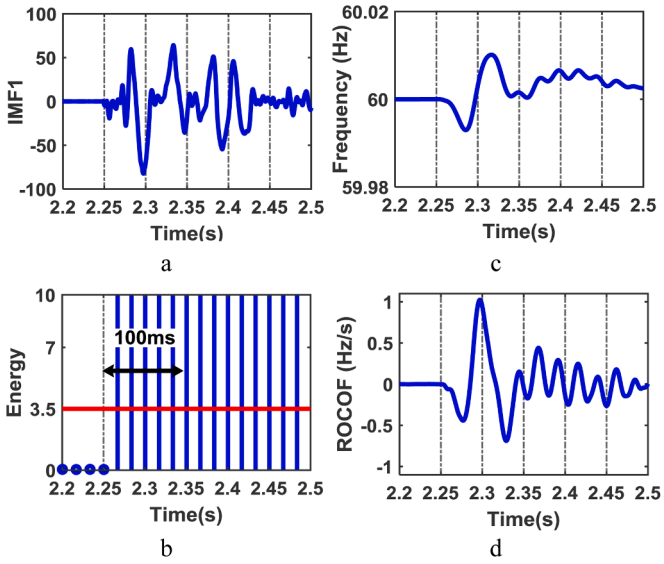

Fig. 6. Performance evaluation under UL 1741 standard, Case 2 (a) first IMF, (b) signal energy of first IMF, (c) frequency, (d) ROCOF.

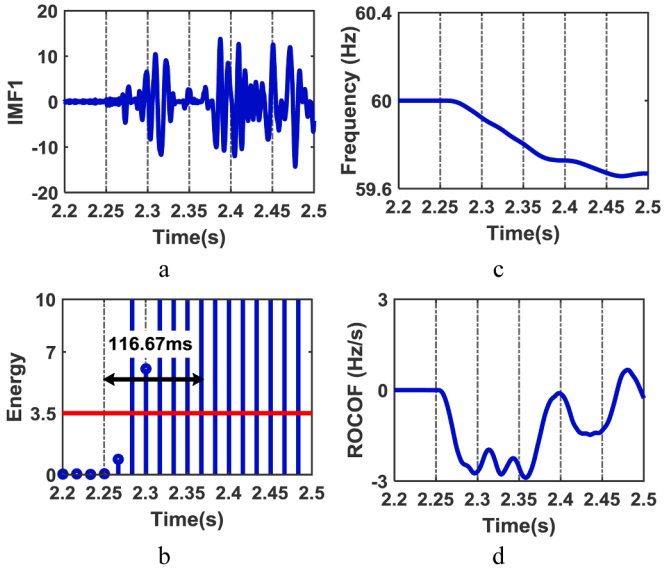

Fig. 7. Performance evaluation under UL 1741 standard, Case 3 (a) first IMF, (b) signal energy of first IMF, (c) frequency, (d) ROCOF.

Table 5
Selected various load for islanding mode test.

No of Cases	Power [Kw]	R [kΩ]	L [H]	C [μF]
4	234	3.282	8.49	0.829
5	246	3.122	8.49	0.829

$$r(t) = x(t) - c(t) \tag{4}$$

$r(t)$ can be considered as new data and by repeating the steps 1 to 7, new IMF component can be obtained.

Step (9): If $r(t)$ contains no more than one extremum, the operation of finding IMF terminates.

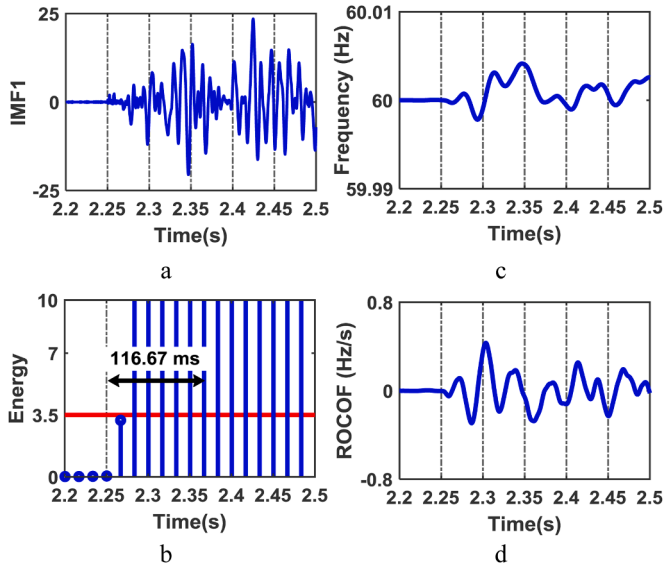

Fig. 8. Performance evaluation for loads in NDZ region, Case 4 (a) first IMF, (b) signal energy of first IMF, (c) frequency, (d) ROCOF.

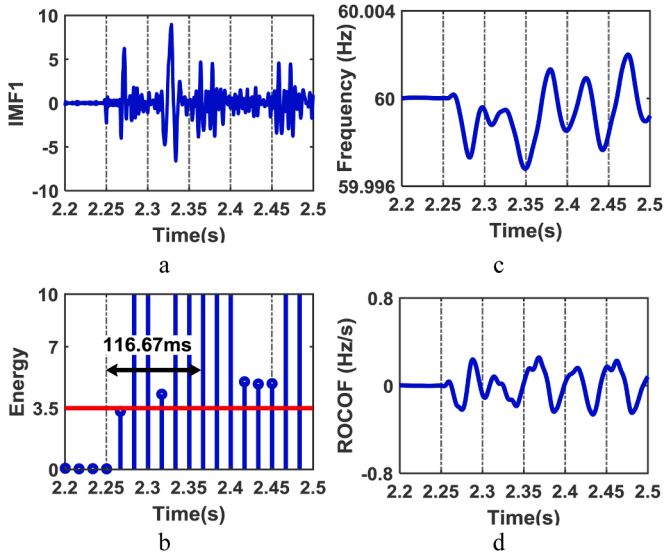

Fig. 9. Performance evaluation for loads in NDZ region, Case 5 (a) first IMF, (b) signal energy of first IMF, (c) frequency, (d) ROCOF.

Table 6
Various nominal loads with different quality factor.

No of Cases	Power [kW]	Quality Factor [Q_f]	R [kΩ]	L [H]	C [μF]
6	240	1.5	3.2	5.66	1.2434
7	240	2.5	3.2	3.39	2.0723

2.2. Positive sequence of voltage signal variations

Assume that v_{abc}(t) denotes the three phase voltage signal at PCC bus of a micro-grid. The voltage signal variations Δv(t) for each phase is defined as follows:

$$\Delta v_a(t) = v_a(t) - v_a(t-\Delta t) \tag{5a}$$

$$\Delta v_b(t) = v_b(t) - v_b(t-\Delta t) \tag{5b}$$

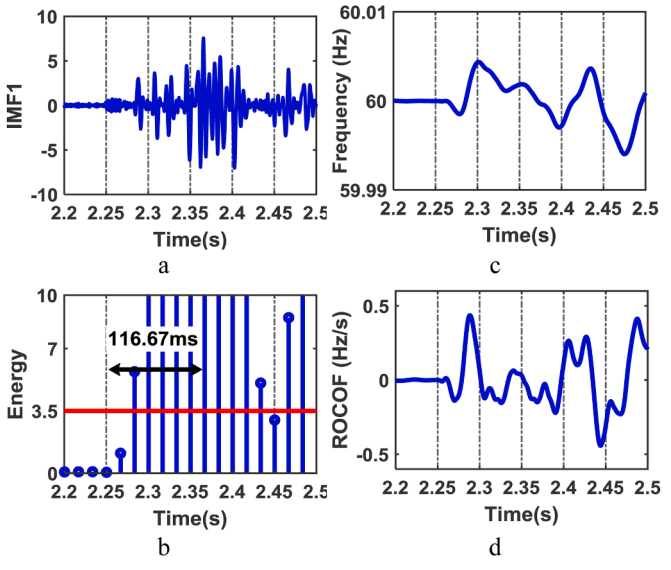

Fig. 10. Performance evaluation for load Quality Factor, Case 6 (a) first IMF, (b) signal energy of first IMF, (c) frequency, (d) ROCOF.

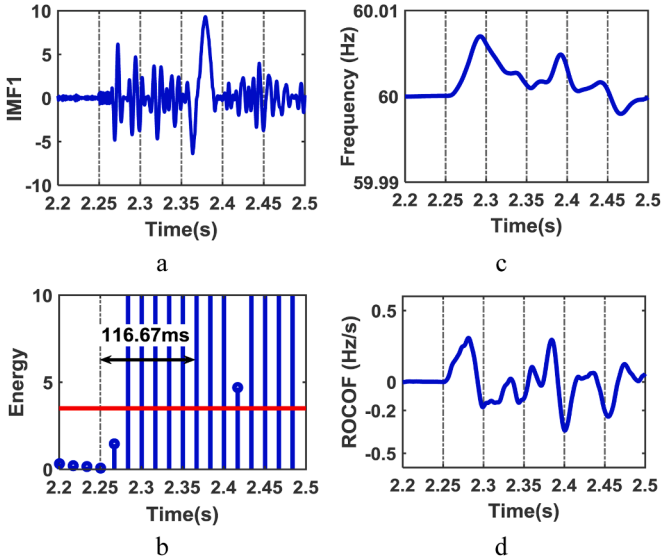

Fig. 11. Performance evaluation for load Quality Factor, Case7 (a) first IMF, (b) signal energy of first IMF, (c) frequency, (d) ROCOF.

Table 7
Evaluation of the method for various load switching.

No of Cases	Type	value
8	Starting induction motor	100 kVA
9	Switching capacitor bank	1 MVAr
10	Closing load	1 MVA
11	Opening load	10 MVA

$$\Delta v_c(t) = v_c(t) - v_c(t-\Delta t) \tag{5c}$$

where $\Delta t = \frac{1}{f_s}$ and f_s is the sampling frequency of the voltage signal and it is selected 10 kHz. In the following, the behavior of Δv in normal operation and islanded mode operation of the microgrid is investigated and furthermore, PSVSV is extracted in both conditions.

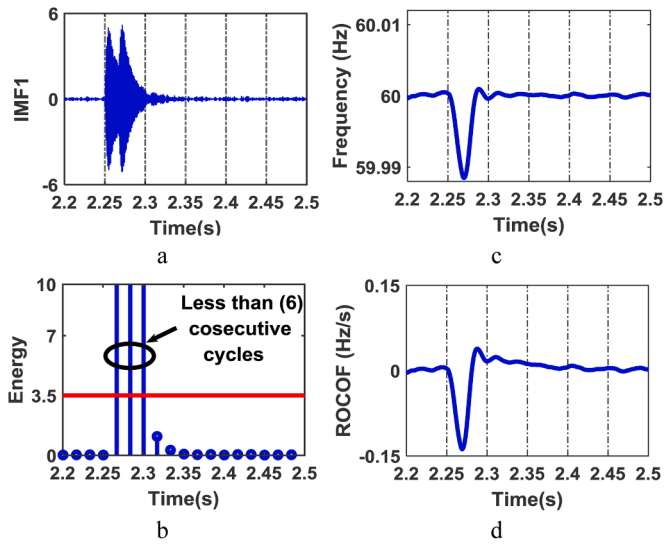

Fig. 12. Performance evaluation for load switching, Case 8 (a) first IMF, (b) signal energy of first IMF, (c) frequency, (d) ROCOF.

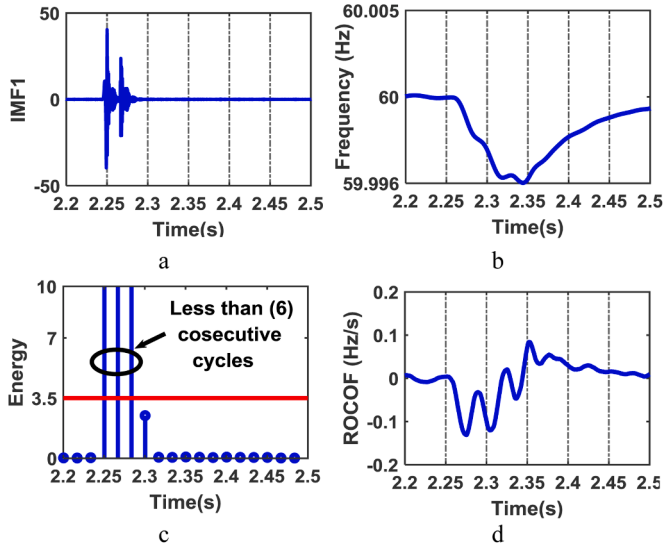

Fig. 13. Performance evaluation for load switching, Case 9 (a) first IMF, (b) signal energy of first IMF, (c) frequency, (d) ROCOF.

2.2.1. *PSVSV under normal operation of the microgrid*

Under normal operation of the microgrid, the three phase voltage signals have balance nature and they are expressed as follows:

$$v_a(t) = V\sin(\omega t) \tag{6a}$$

$$v_b(t) = Vsin\left(\omega t - \frac{2\pi}{3}\right) \tag{6b}$$

$$v_c(t) = Vsin\left(\omega t + \frac{2\pi}{3}\right) \tag{6c}$$

According to (5a), $\Delta v_a(t)$ is calculated as follows:

$$\Delta v_a(t) = v_a(t) - v_a(t-\Delta t) = Vsin(\omega t) - Vsin(\omega t - \omega\Delta t)$$
$$= 2Vcos\left(\omega t - \frac{\omega\Delta t}{2}\right)\sin\left(\frac{\omega\Delta t}{2}\right) \tag{7a}$$

Similar to $\Delta v_a(t)$, the following expressions can be concluded for $\Delta v_b(t)$ and $\Delta v_c(t)$ as follows:

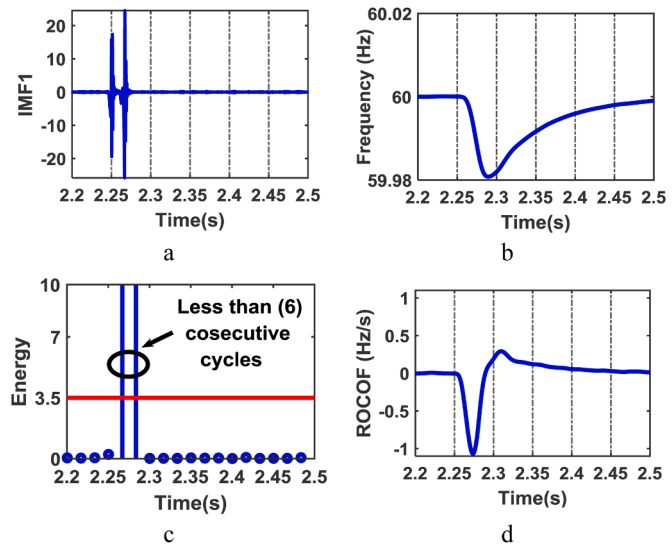

Fig. 14. Performance evaluation for load switching, Case 10 (a) first IMF, (b) signal energy of First IMF, (c) frequency, (d) ROCOF.

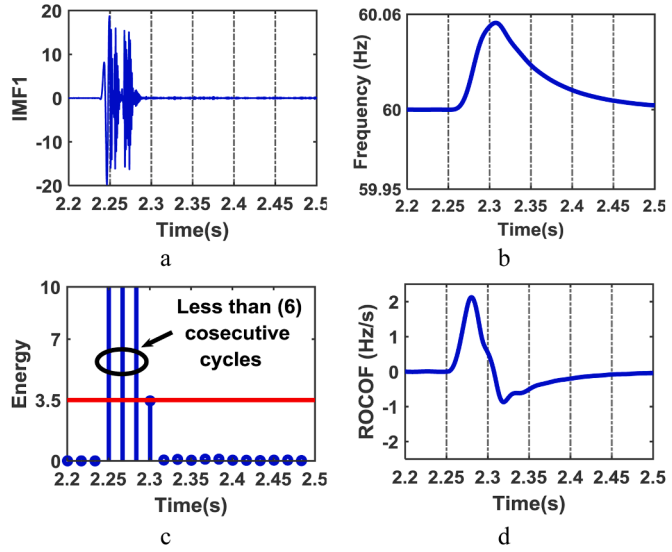

Fig. 15. Performance evaluation for load switching, Case 11 (a) first IMF, (b) signal energy of First IMF, (c) frequency, (d) ROCOF.

Table 8
Cases with different fault.

No of Cases	Type	R_f [Ω]
12	LG	0.05
13	LLG	0.05
14	LLLG	0.05
15	LLLG	30

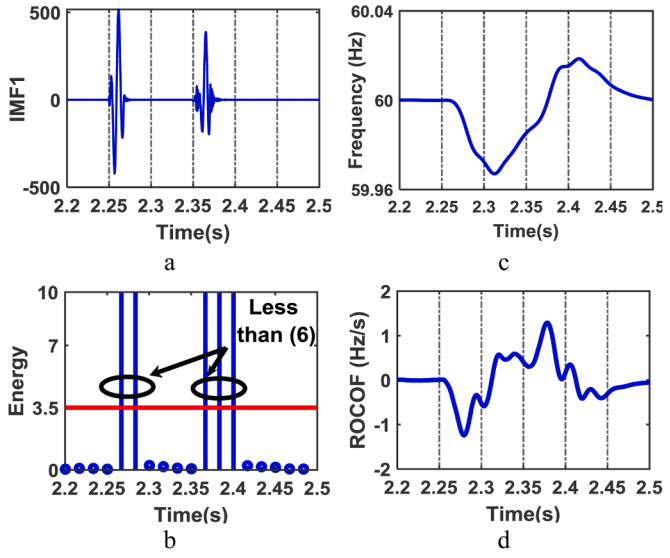

Fig. 16. Performance evaluation for short circuit faults, Case 12 (a) first IMF, (b) signal energy of first IMF, (c) frequency, (d) ROCOF.

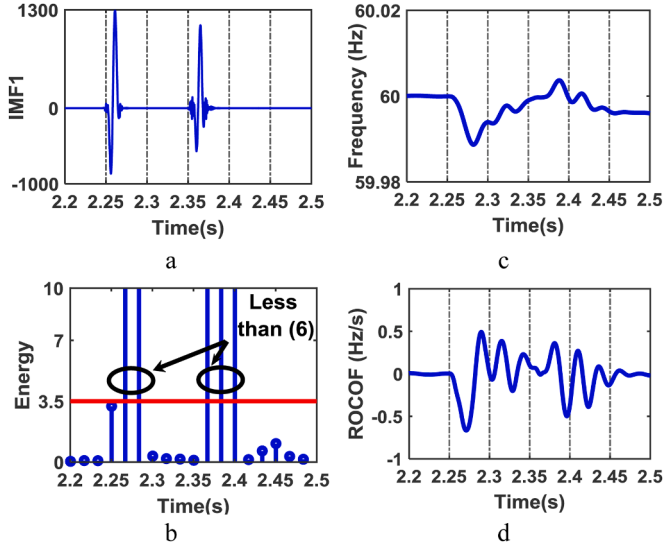

Fig. 17. Performance evaluation for short circuit faults, Case 13 (a) first IMF, (b) signal energy of first IMF, (c) frequency, (d) ROCOF.

$$\Delta v_b(t) = 2Vcos\left(\omega t - \frac{\omega\Delta t}{2} - \frac{2\pi}{3}\right)\sin\left(\frac{\omega\Delta t}{2}\right) \tag{7b}$$

$$\Delta v_c(t) = 2Vcos\left(\omega t - \frac{\omega\Delta t}{2} + \frac{2\pi}{3}\right)\sin\left(\frac{\omega\Delta t}{2}\right) \tag{7c}$$

Under normal operation of the microgrid, ω has constant value and as a result, $\sin\left(\frac{\omega\Delta t}{2}\right)$ has a constant value.

The phasor of $\Delta v_a(t)$, $\Delta v_b(t)$, and $\Delta v_c\ (t)$ are as follows:

$$\Delta V_a = \left(2V\sin\left(\frac{\omega\Delta t}{2}\right)\right)\left(-\frac{\omega\Delta t}{2}\right) = \left(2V\sin\left(\frac{\omega\Delta t}{2}\right)\right)e^{\left(-j\frac{\omega\Delta t}{2}\right)} \tag{8a}$$

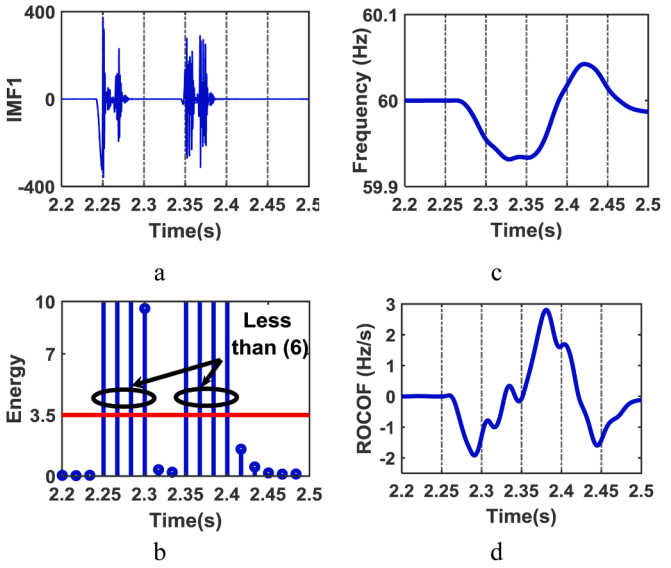

Fig. 18. Performance evaluation for short circuit faults, Case 14 (a) first IMF, (b) signal energy of first IMF, (c) frequency, (d) ROCOF.

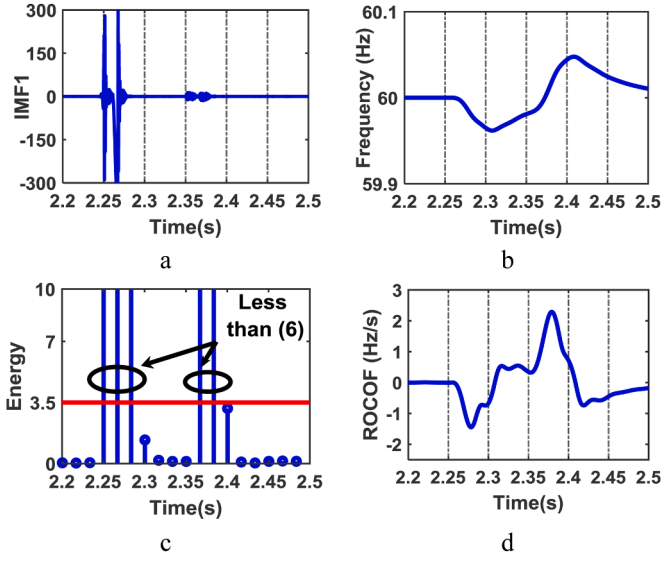

Fig. 19. Performance evaluation for short circuit faults, Case 15 (a) first IMF, (b) signal energy of first IMF, (c) frequency, (d) ROCOF.

$$\Delta V_b = \left(2V\sin\left(\frac{\omega\Delta t}{2}\right)\right)\left(-\frac{\omega\Delta t}{2} - \frac{2\pi}{3}\right) = \left(2V\sin\left(\frac{\omega\Delta t}{2}\right)\right)e^{\left(-j\frac{\omega\Delta t}{2} - j\frac{2\pi}{3}\right)} \tag{8b}$$

$$\Delta V_c = \left(2V\sin\left(\frac{\omega\Delta t}{2}\right)\right)\left(-\frac{\omega\Delta t}{2} + \frac{2\pi}{3}\right) = \left(2V\sin\left(\frac{\omega\Delta t}{2}\right)\right)e^{\left(-j\frac{\omega\Delta t}{2} + j\frac{2\pi}{3}\right)} \tag{8c}$$

Considering $\alpha = e^{j\frac{2\pi}{3}}$, the positive sequence of ΔV_a, ΔV_b, and $\Delta V_c$are calculated as follows:

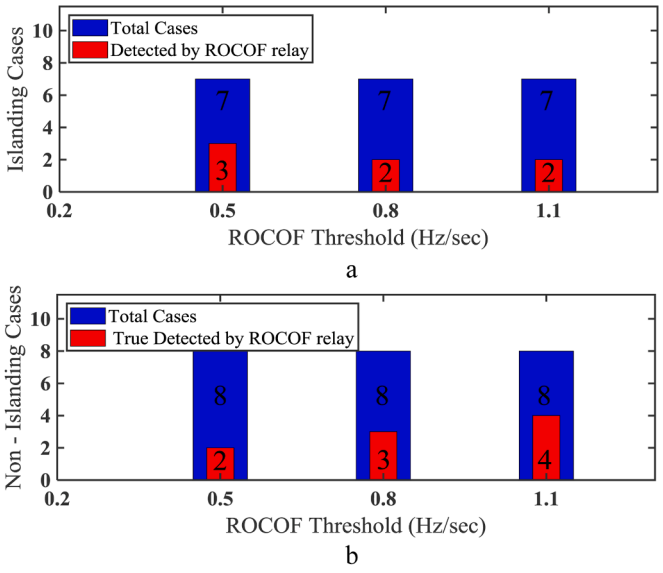

Fig. 20. Various ROCOF settings for (a) islanding event, (b) non-islanding event.

Table 9
Selected various load type for islanding mode test.

Load Type	Case Number	Power (KW)	△P (%)
Constant P	Case 16	240	0
	Case 17	264	10
Constant I	Case 18	240	0
	Case 19	264	10

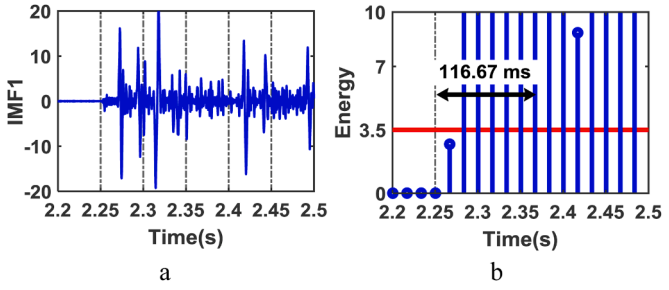

Fig. 21. Performance evaluation for case 16, (a) first IMF, (b) signal energy of first IMF.

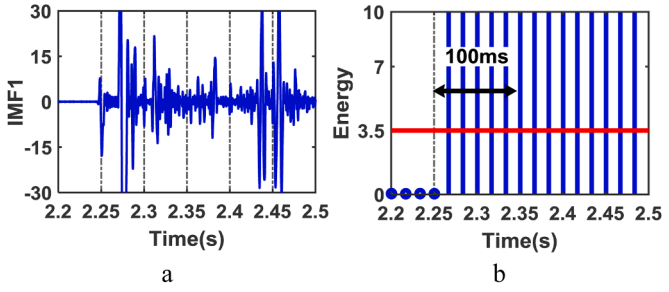

Fig. 22. Performance evaluation for case 17, (a) first IMF, (b) signal energy of first IMF.

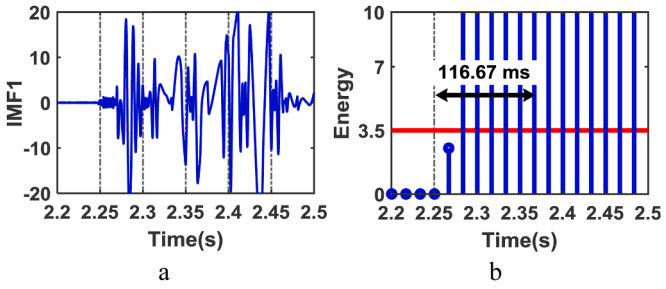

Fig. 23. Performance evaluation for case 18, (a) first IMF, (b) signal energy of first IMF.

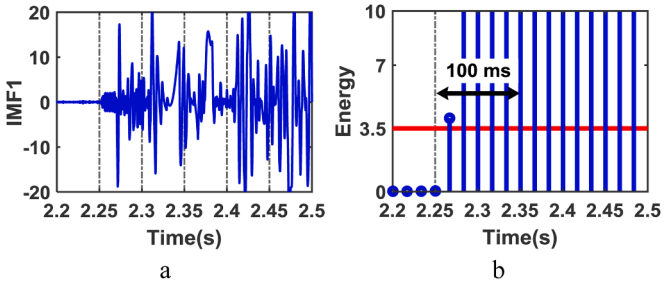

Fig. 24. Performance evaluation for case 19, (a) first IMF, (b) signal energy of first IMF.

$$\Delta V^{+} = \frac{1}{3}\left[\Delta V_a + \alpha \times \Delta V_b + \alpha^2 \times \Delta V_c\right]$$
$$= \frac{1}{3}\frac{1}{3}\left[\left(2V\sin\left(\frac{\omega\,\Delta t}{2}\right)\right)e^{\left(-j\frac{\omega\,\Delta t}{2}\right)} + \left(2V\sin\left(\frac{\omega\,\Delta t}{2}\right)\right)e^{\left(-j\frac{\omega\,\Delta t}{2} - j\frac{2\pi}{3}\right)} \times e^{j\frac{2\pi}{3}} + \left(2V\sin\left(\frac{\omega\,\Delta t}{2}\right)\right)e^{\left(-j\frac{\omega\,\Delta t}{2} + j\frac{2\pi}{3}\right)} \times e^{-j\frac{2\pi}{3}}\right]$$
$$= \left(2V\sin\left(\frac{\omega\,\Delta t}{2}\right)\right)e^{\left(-j\frac{\omega\,\Delta t}{2}\right)} \quad (9)$$

where ΔV^{+} denotes positive sequence of ΔV_a, ΔV_b and ΔV_c. Having ΔV^{+}, PSVSV is calculated as follows:

$$PSVSV = |\Delta V^{+}| = 2V\sin\left(\frac{\omega\,\Delta t}{2}\right) \quad (10)$$

2.2.2. PSVSV under islanded operation of the microgrid

Under islanded operation of the microgrid, the three phase voltage signals have unbalance nature and they are expressed as follows:

$$v_a(t) = V_{1t}\sin(\omega_t t) \quad (11a)$$

$$v_b(t) = V_{2t}\sin(\omega_t t - 2\pi/3) \quad (11b)$$

$$v_c(t) = V_{3t}\sin(\omega_t t + 2\pi/3) \quad (11c)$$

where, V_t and ω_t denote time-variant behavior of voltage magnitude and frequency respectively. Same as previous subsection, $\Delta v_a(t)$ is calculated as follows:

$$\Delta v_a(t) = v_a(t) - v_a(t - \Delta t) = V_{1t}sin(\omega_t t) - V_{1t}sin(\omega_t t - \omega_t\,\Delta t)$$
$$= 2V_{1t}cos\left(\omega_t t - \frac{\omega_t\,\Delta t}{2}\right)\sin\left(\frac{\omega_t\,\Delta t}{2}\right) \quad (12)$$

Assuming $V_{1t} = V_{2t} = V_{3t} = V_t$, PSVSV is calculated as follows:

$$PSVSV = |\Delta V^{+}| = 2V_t sin\left(\frac{\omega_t\,\Delta t}{2}\right) \quad (13)$$

Table 10
Performance evaluation of the proposed method for different types of loads.

△P %	△Q %	Maximum number of consecutive cycles larger than 3.5		
		Constant Z	Constant I	Constant P
-30	-20	14	14	14
	-15	14	14	14
	-10	14	14	14
	-5	14	14	14
	0	14	14	14
	5	14	14	14
	10	14	14	14
	15	14	14	14
	20	14	14	14
-20	-20	14	14	14
	-15	14	14	14
	-10	14	14	14
	-5	14	14	14
	0	14	14	14
	5	14	14	14
	10	14	14	14
	15	14	14	14
	20	14	14	14
-10	-20	14	14	14
	-15	14	14	14
	-10	14	14	14
	-5	14	14	14
	0	14	14	14
	5	14	14	14
	10	14	14	14
	15	14	14	14
	20	14	14	14
0	-20	14	14	14
	-15	14	14	14
	-10	14	14	14
	-5	14	14	14
	0	12	13	13
	5	14	14	14
	10	14	14	14
	15	14	14	14
	20	14	14	14
10	-20	14	14	14
	-15	14	14	14
	-10	14	14	14
	-5	14	14	14
	0	14	14	14
	5	14	14	14
	10	14	14	14
	15	14	14	14
	20	14	14	14
20	-20	14	14	14
	-15	14	14	14
	-10	14	14	14
	-5	14	14	14
	0	14	14	14
	5	14	14	14
	10	14	14	14
	15	14	14	14
	20	14	14	14
30	-20	14	14	14
	-15	14	14	14
	-10	14	14	14
	-5	14	14	14
	0	14	14	14
	5	14	14	14
	10	14	14	14
	15	14	14	14
	20	14	14	14

2.3. Calculating signal energy of First IMF of PSVSV

The energy of signal is defined as the integral of the absolute squares of the signal over one fundamental period T. The signal energy of first IMF of PSVSV (IPSVSV) is mathematically calculated as follows:

$$SE = \frac{1}{T}\int^{|IPSVSV|^2} dt \tag{14}$$

where, SE is signal energy.

2.4. Implementation of proposed algorithm

The procedure of the proposed algorithm is shown in Fig. 1. The steps of the proposed method algorithm are as follows:

1) The voltage signals at PCC bus are obtained. The frequency of the sampling rate is selected 10 kHz.
2) Calculating ΔV_a, ΔV_b and ΔV_c for obtaining ΔV^+ using (9).
3) *PSVSV* is calculated using (10).
4) *IPSVSV* is calculated according to Section 2.1.
5) Using (14), the signal energy of *IPSVSV* is calculated. Note that the islanding is identified if SE becomes more than threshold for 6 consecutive cycles.

3. Simulation results and discussions

To evaluate the performance of the proposed algorithm, a microgrid is simulated in MATLAB as shown in Fig. 2. The specification of the microgrid are provided in Table 2. The test system contains a 240 kW PV panel and the microgrid becomes islanded once circuit breaker opens at t = 2.25 s. In this model, a constant current controlled type of inverter has been utilized. The inverter's control system consists of five major subsystems which are described in the following. Note that the block diagrams of the control systems are provided in the appendix.

1) The Maximum Power Point Tracking (MPPT) controller which is based on the 'Perturb and Observe' (P&O) technique. This MPPT system automatically varies the V_{DC} reference signal of the inverter V_{DC} regulator in order to obtain a DC voltage which will extract maximum power from the PV array, based on the following equation:

$$V_{DC,ref}(k) = V_{DC,ref}(k-1) + \alpha \cdot \text{sign}\left(\frac{\partial P_{PV}}{\partial V_{PV}}(k)\right) \tag{15}$$

where k, k-1 are consecutive time steps, $\alpha > 0$ is an increment value used to increase/decrease $V_{DC,ref}$, and the function sign(x) is defined as follows:

$$sign(x) = \begin{cases} 1 & if\ x > 0 \\ -1 & if\ x < 0 \end{cases} \tag{16}$$

This method is relatively simple [43], knowledge of the characteristics of the photovoltaic array is not required. The flowchart of MPPT is shown in appendix.

1) V_{DC} Regulator for determining the required Id (active current) reference for the current regulator.
2) Current Regulator for determining the required reference voltages for the inverter based on the current references Id and Iq (reactive current). In this model, the Iq reference is set to zero.
3) PLL and Measurements which is required for synchronization and voltage/current measurements.
4) PWM Generator for Generating firing signals to the IGBTs based on the required reference voltages. In our example, the carrier frequency is set to 1980 Hz (33*60). The block diagrams and constant parameters of the constant current controlled inverter and its major subsystems are shown in appendix.

Fig. 3 shows the magnitude and frequency of the voltage signal at PCC bus of the microgrid. According to Fig. 3, after breaker operation

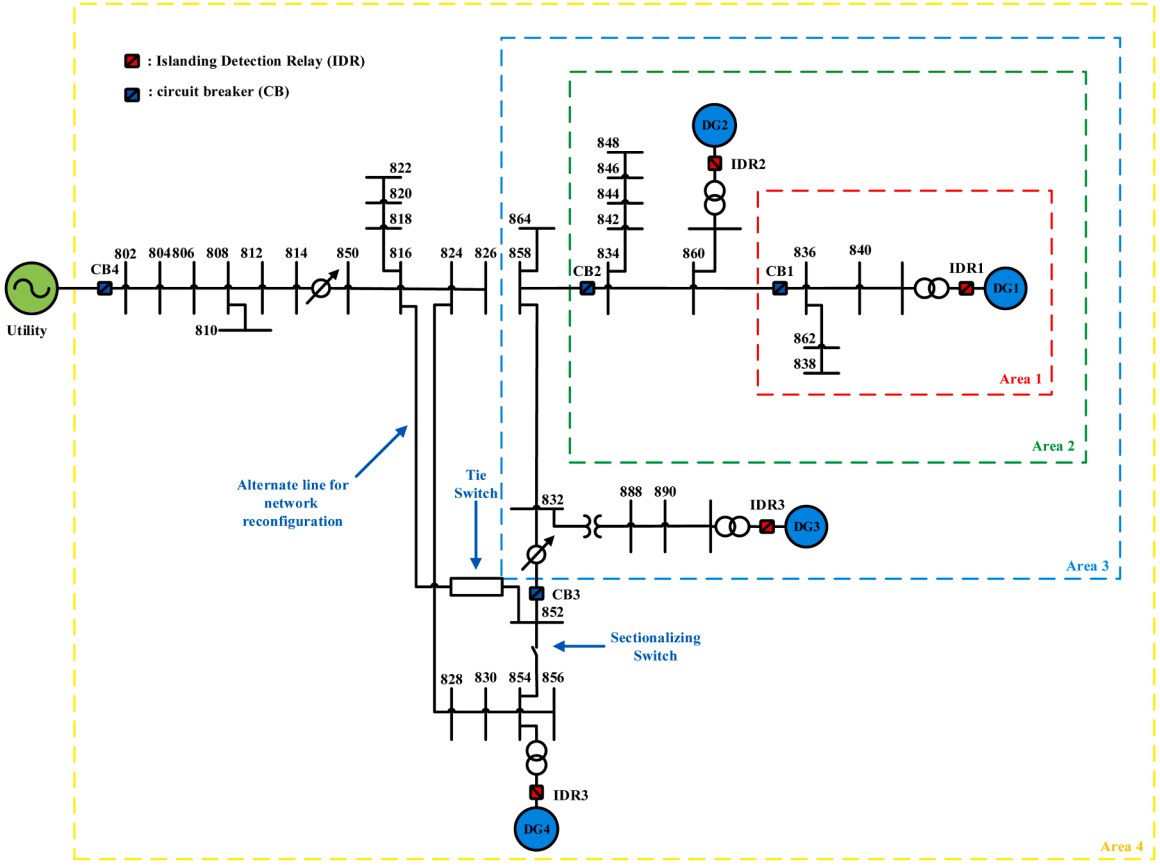

Fig. 25. Single-line diagram of IEEE 34 bus network.

Table 11
Specifications of each area.

Area	Island formation
1	network contains DG1
2	network contains DG1, DG2
3	network contains DG1, DG2, DG3
4	network contains DG1, DG2, DG3 and DG4

and turning to islanding mode, even considering full balance between load and generation, the magnitude and frequency of the signal have time-variant behavior. As a result, the PSVSV and first IMF show time-variant behavior during islanding mode of the microgrid. Therefore, energy signal of first IMF can be employed for islanding detection in the microgrid.

3.1. Selecting the threshold

Except islanding, there are some circumstances that the islanding detection algorithm should be able to deal with them including short circuit fault condition, load switching, motor starting and capacitor bank switching. As a result, it is essential to select a proper threshold to discriminate islanding from other circumstances considering reliability in correct operation and simultaneously preserving speed of detection. To such aim, an algorithm named "*Otsu thresholding method*" has been utilized which is a well-known and reliable method, employed in different engineering fields [44–48]. In the following, implementation of *Otsu thresholding method* in the proposed method is described in more details.

1) In the first step, a Probability Function Density (PDF) is assigned to a desired parameter for different conditions such as islanding and non-islanding scenarios which are tabulated in Table 3. (in the proposed method, PDFs should be assigned for index SE)
2) In the second step, a normal function based curve should be fitted for each case.
3) In the third step, the intersection point of the PDF curves regarding the islanding and non-islanding cases is selected as the threshold value.

To implement the *Otsu thresholding method* in the proposed method, distribution fitting tool (DFITTOOL) toolbox in MATLAB has been utilized. As one can see in Fig. 4, the PDF of the SE for islanding and non-islanding have intersection at 3.5. As a result, 3.5 is considered as the threshold. Note that, during calculation of SE, the voltage signals are assumed to be per unit. As a result, the calculation of SE only depends on the variations of PSVSV.

As it can be seen in Fig. 4, the SE for non-islanding conditions may have much higher value than 3.5. As discussed in the paper, we considered an extra criterion (i.e. 6 consecutive cycles of SE) for decision making. In other words, if the SE remains higher than 3.5 for 6 consecutive cycles of SE, the islanding is detected. On the contrary, if the SE does not remain higher than 3.5 for 6 consecutive cycles of SE, the condition is not considered as an islanding case.

3.2. Performance evaluation under UL 1741 standard

In this section, the performance of the proposed algorithm is evaluated based on the UL 1741 Standard. Based on this standard [49], the load's active power varies between 25, 50, 100, and 125 % of the output active power of the PV's inverter. Also, during the test, the load's reactive power is allowed to change between 95% to 105% with step

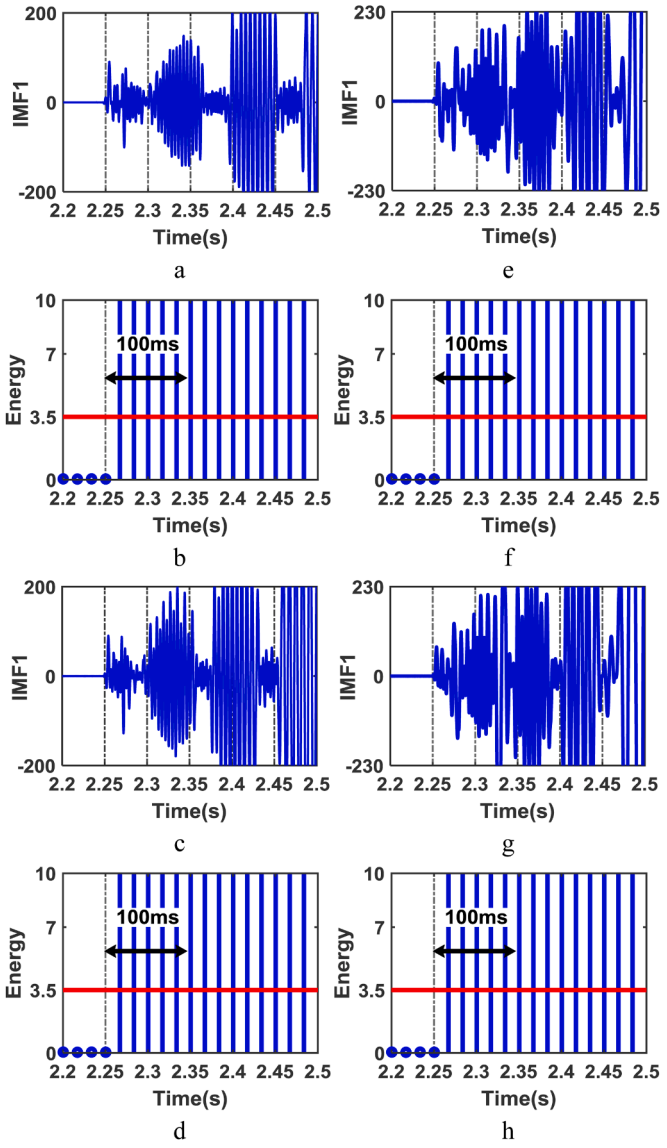

Fig. 26. Simulation result for islanding in area 4 in IEEE 34 bus distribution network, (a) first IMF of DG1, (b) signal energy of first IMF of DG1, (c) first IMF of DG2, (d) signal energy of first IMF of DG2, (e) first IMF of DG3, (f) signal energy of first IMF of DG3, (g) first IMF of DG4, (h) signal energy of first IMF of DG4.

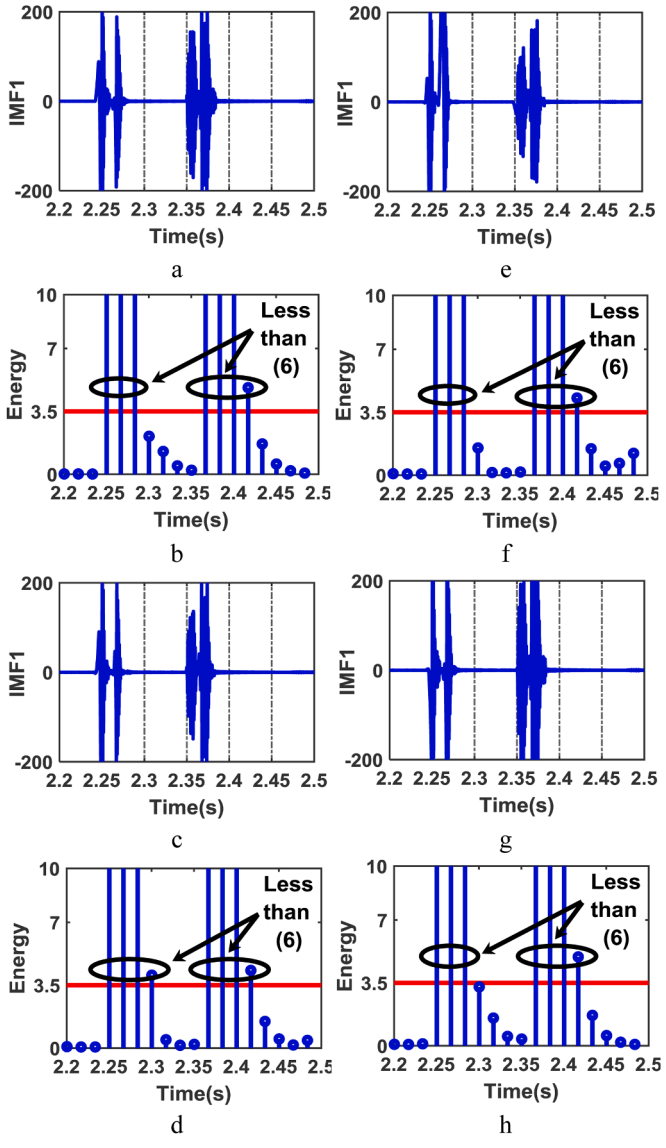

Fig. 27. Simulation result for three phase fault in IEEE 34 bus distribution network, (a) first IMF of DG1, (b) signal energy of First IMF of DG1, (c) first IMF of DG2, (d) signal energy of First IMF of DG2, (e) first IMF of DG3, (f) signal energy of First IMF of DG3, (g) first IMF of DG4, (h) signal energy of First IMF of DG4.

equal to 1% while the power factor should be remained unity. Some conditions for applying this test are provided in Table 4. As it can be seen in Fig. 5, once breaker operates at t=2.25 s, the frequency and ROCOF remain in allowable ranges since in this condition it is assumed that full balance exists between load and generation. However, proposed index shows variation in SE higher than threshold for at least 6 consecutive cycles and as a result, the proposed method successfully identify islanding. Note that for case 1 shown in Fig. 6, the islanding is detected 116.67 ms after breaker opening. As shown in Figs. 6 and 7 and according to cases 2 and 3, with enhancing the level of unbalance between load and generation, the proposed index can even identify the islanding faster than full balance condition.

3.3. *Performance evaluation for loads in NDZ region of voltage and frequency relays*

The main bottleneck for islanding detection is the formation of regions within the grid where the adopted method is unable to operate, i.e., NDZ. For the inverter-based DG systems, NDZ is determined according to the control strategy of inverter based active and reactive power mismatches. In this investigation, the NDZ of voltage and frequency relays are adopted from [11]. It is assumed that the allowable operating voltage range is between 0.88 to 1.1 per unit. As a result, according to [11], the unbalance level of active power corresponding to the allowable operating voltage range is between -24 kW to 28.8 kW

Table 12
Results of proposed method for islanding conditions in IEEE 34 bus network.

Islanding Area	Maximum number of consecutive cycle of SE larger than 3.5			
	DG1	DG2	DG3	DG4
IEEE 34 bus network				
Area 1	14	14	14	14
Area 2	14	14	14	14
Area 3	14	14	14	14
Area 4	14	14	14	14

Table 13
Results of proposed method for islanding conditions in IEEE 34 bus network after reconfiguration.

Islanding Area	Maximum number of consecutive cycle of SE larger than 3.5			
	DG1	DG2	DG3	DG4
IEEE 34 bus network after reconfiguration				
Area 1	14	14	14	14
Area 2	14	14	14	14
Area 3	14	14	14	14
Area 4	14	14	14	14

respectively. Also, considering nominal frequency 60 Hz, the allowable range of frequency deviation is between 59.3 Hz to 60.5 Hz. Therefore, according to [11], unbalance level of reactive power is between -5.7 kVAr and 3.95 kVAr. Some cases are provided in Table 5 to evaluate the performance of the proposed algorithm for load variation in NDZ region of voltage and frequency relays. It should be noted that in all cases, the frequency and ROCOF remain in the allowable range of variations. As a result, the conventional frequency and voltage relays are unable to detect islanding in the aforementioned circumstances. In this investigation, it has been assumed that while the active power has some level of unbalance, the reactive power of the load has full balance which result in difficult situation in islanding detection. According to Table 5, the unbalance level of active power is selected to -6 kW and 6 kW considering full balance in reactive power. After breaker opening at t=2.25 s, the microgrid becomes islanded and as it can be seen in Figs. 8 and 9, the ROCOF remains in allowable range of variations. However, the proposed index shows islanding is detected since it takes values more than threshold for at least 6 consecutive cycles of energy.

3.4. Performance evaluation for load quality factor

Large quality factor Q_f in parallel RLC loads may challenge the performance of the islanding detection algorithms especially shifting frequency based algorithms. This section investigates the performance of the proposed index under nominal load condition for different Q_f . This investigation is conducted under full balance between load and generation. Also, based on UL 1741 standard, Q_f should be less than 2.5. According to Table 6, some Q_f are provided for a RLC load to investigate the performance of the proposed index. As one can see in Figs. 10 and 11, while ROCOF shows no violation in allowable frequency variation, the proposed index successfully detects islanding after 116.67 ms.

3.5. Performance evaluation for load switching

According to Table 7, the performance of the proposed algorithm for different linear and nonlinear load switching are evaluated in this section. As it can be seen in the Figs. 12–15, ROCOF fails to detect non-islanded condition since the frequency variations becomes larger than the allowable range. However, the proposed index does not satisfy the islanding criterion and it reaches below the threshold before 6 consecutive cycles of energy. As a result, the proposed algorithm, is able to distinguish non-islanding condition even in the case of load switching condition.

3.6. Performance evaluation for short circuit faults

According to Table 8, the proposed algorithm is evaluated for different short circuit faults. The fault is initiated at t=2.25 s, and it remains for 0.1 s. according to Figs. 16–19, ROCOF fails to discriminate non-islanding from islanding condition since the frequency variations exceed allowable range. However, the proposed index does not satisfy the islanding criterion and it reaches below the threshold before 6 consecutive cycles of energy. Note that as the fault resistance increased, the SE samples greater than the threshold is decreased. As a result, the proposed algorithm, is able to distinguish fault condition from islanding condition.

Table 14
Results of proposed method for non- islanding conditions in IEEE 34 bus network.

Type	Parameter	Location	Maximum number of consecutive cycle of SE larger than 3.5			
			DG1	DG2	DG3	DG4
IEEE 34 bus network						
LG	25% of	$R_f = 1\ \Omega$	4	4	4	4
	Feeder1	$R_f = 10\ \Omega$	4	4	4	4
	50% of	$R_f = 1\ \Omega$	4	4	4	4
	Feeder1	$R_f = 10\ \Omega$	4	4	4	4
	75% of	$R_f = 1\ \Omega$	4	4	4	4
	Feeder1	$R_f = 10\ \Omega$	4	4	4	4
	100% of	$R_f = 1\ \Omega$	4	4	4	4
	Feeder1	$R_f = 10\ \Omega$	4	4	4	4
	25% of	$R_f = 1\ \Omega$	4	4	4	4
	Feeder2	$R_f = 10\ \Omega$	4	4	4	4
	50% of	$R_f = 1\ \Omega$	4	4	4	4
	Feeder2	$R_f = 10\ \Omega$	4	4	4	4
	75% of	$R_f = 1\ \Omega$	4	4	4	4
	Feeder2	$R_f = 10\ \Omega$	4	4	4	4
	100% of	$R_f = 1\ \Omega$	4	4	4	4
	Feeder2	$R_f = 10\ \Omega$	4	4	4	4
LLG	25% of	$R_f = 1\ \Omega$	4	4	4	4
	Feeder1	$R_f = 10\ \Omega$	4	4	4	4
	50% of	$R_f = 1\ \Omega$	4	4	4	4
	Feeder1	$R_f = 10\ \Omega$	4	4	4	4
	75% of	$R_f = 1\ \Omega$	4	4	4	4
	Feeder1	$R_f = 10\ \Omega$	4	4	4	4
	100% of	$R_f = 1\ \Omega$	4	4	4	4
	Feeder1	$R_f = 10\ \Omega$	4	4	4	4
	25% of	$R_f = 1\ \Omega$	4	4	4	4
	Feeder2	$R_f = 10\ \Omega$	4	4	4	4
	50% of	$R_f = 1\ \Omega$	4	4	4	4
	Feeder2	$R_f = 10\ \Omega$	4	4	4	4
	75% of	$R_f = 1\ \Omega$	4	4	4	4
	Feeder2	$R_f = 10\ \Omega$	4	4	4	4
	100% of	$R_f = 1\ \Omega$	4	4	4	4
	Feeder2	$R_f = 10\ \Omega$	4	4	4	4
LLLG	25% of	$R_f = 1\ \Omega$	4	4	4	4
	Feeder1	$R_f = 10\ \Omega$	4	4	4	4
	50% of	$R_f = 1\ \Omega$	4	4	4	4
	Feeder1	$R_f = 10\ \Omega$	4	4	4	4
	75% of	$R_f = 1\ \Omega$	4	4	4	4
	Feeder1	$R_f = 10\ \Omega$	4	4	4	4
	100% of	$R_f = 1\ \Omega$	4	4	4	4
	Feeder1	$R_f = 10\ \Omega$	4	4	4	4
	25% of	$R_f = 1\ \Omega$	4	4	4	4
	Feeder2	$R_f = 10\ \Omega$	4	4	4	4
	50% of	$R_f = 1\ \Omega$	4	4	4	4
	Feeder2	$R_f = 10\ \Omega$	4	4	4	4
	75% of	$R_f = 1\ \Omega$	4	4	4	4
	Feeder2	$R_f = 10\ \Omega$	4	4	4	4
	100% of	$R_f = 1\ \Omega$	4	4	4	4
	Feeder2	$R_f = 10\ \Omega$	4	4	4	4
Switching Capacitor bank	Bus 832	1000 kVAr	2	2	3	3
	Bus 834	1000 kVAr	3	3	3	3
	Bus 836	1000 kVAr	3	3	3	3
Starting Induction Motor	Bus 832	1000 Kva	2	2	2	2
	Bus 834	1000 kVA	2	3	2	2
	Bus 836	1000 kVA	3	3	3	3

3.7. Performance evaluation of ROCOF relay for cases 1-15

Fig. 20 shows the performance of the ROCOF algorithm for given 15 cases considering various islanding and non-islanding conditions. Note that ROCOF relay may have different setting (e.g. 0.5, 0.8, and 1.1 according to [50,51]). According to Fig. 20a, simulation results indicate

Table 15
Results of proposed method for non- islanding conditions in IEEE 34 bus network after reconfiguration.

Type	Parameter	Location	Maximum number of consecutive cycle of SE larger than 3.5			
			DG1	DG2	DG3	DG4
IEEE 34 bus network after reconfiguration						
LG	25% of	$R_f = 1\ \Omega$	4	4	4	4
	Feeder1	$R_f = 10\ \Omega$	4	4	4	4
	50% of	$R_f = 1\ \Omega$	4	4	4	4
	Feeder1	$R_f = 10\ \Omega$	4	4	4	4
	75% of	$R_f = 1\ \Omega$	4	4	4	4
	Feeder1	$R_f = 10\ \Omega$	4	4	4	4
	100% of	$R_f = 1\ \Omega$	4	4	4	4
	Feeder1	$R_f = 10\ \Omega$	4	4	4	4
	25% of	$R_f = 1\ \Omega$	4	4	4	4
	Feeder2	$R_f = 10\ \Omega$	4	4	4	4
	50% of	$R_f = 1\ \Omega$	4	4	4	4
	Feeder2	$R_f = 10\ \Omega$	4	4	4	4
	75% of	$R_f = 1\ \Omega$	4	4	4	4
	Feeder2	$R_f = 10\ \Omega$	4	4	4	4
	100% of	$R_f = 1\ \Omega$	4	4	4	4
	Feeder2	$R_f = 10\ \Omega$	4	4	4	4
LLG	25% of	$R_f = 1\ \Omega$	4	4	4	4
	Feeder1	$R_f = 10\ \Omega$	4	4	4	4
	50% of	$R_f = 1\ \Omega$	4	4	4	4
	Feeder1	$R_f = 10\ \Omega$	4	4	4	4
	75% of	$R_f = 1\ \Omega$	4	4	4	4
	Feeder1	$R_f = 10\ \Omega$	4	4	4	4
	100% of	$R_f = 1\ \Omega$	4	4	4	4
	Feeder1	$R_f = 10\ \Omega$	4	4	4	4
	25% of	$R_f = 1\ \Omega$	4	4	4	4
	Feeder2	$R_f = 10\ \Omega$	4	4	4	4
	50% of	$R_f = 1\ \Omega$	4	4	4	4
	Feeder2	$R_f = 10\ \Omega$	4	4	4	4
	75% of	$R_f = 1\ \Omega$	4	4	4	4
	Feeder2	$R_f = 10\ \Omega$	4	4	4	4
	100% of	$R_f = 1\ \Omega$	4	4	4	4
	Feeder2	$R_f = 10\ \Omega$	4	4	4	4
LLLG	25% of	$R_f = 1\ \Omega$	4	4	4	4
	Feeder1	$R_f = 10\ \Omega$	4	4	4	4
	50% of	$R_f = 1\ \Omega$	4	4	4	4
	Feeder1	$R_f = 10\ \Omega$	4	4	4	4
	75% of	$R_f = 1\ \Omega$	4	4	4	4
	Feeder1	$R_f = 10\ \Omega$	4	4	4	4
	100% of	$R_f = 1\ \Omega$	4	4	4	4
	Feeder1	$R_f = 10\ \Omega$	4	4	4	4
	25% of	$R_f = 1\ \Omega$	4	4	4	4
	Feeder2	$R_f = 10\ \Omega$	4	4	4	4
	50% of	$R_f = 1\ \Omega$	4	4	4	4
	Feeder2	$R_f = 10\ \Omega$	4	4	4	4
	75% of	$R_f = 1\ \Omega$	4	4	4	4
	Feeder2	$R_f = 10\ \Omega$	4	4	4	4
	100% of	$R_f = 1\ \Omega$	4	4	4	4
	Feeder2	$R_f = 10\ \Omega$	4	4	4	4
Switching Capacitor bank	Bus 832	1000 kVAr	2	2	3	3
	Bus 834	1000 kVAr	2	2	3	3
	Bus 836	1000 kVAr	3	2	3	3
Starting Induction Motor	Bus 832	1000 kVA	2	2	2	2
	Bus 834	1000 kVA	2	3	2	2
	Bus 836	1000 kVA	3	3	3	3

Table 16
Load conditions for 3 cases.

Case	Linear load (%)	Non-linear load (%)
20	100	0
21	80	20
22	60	40

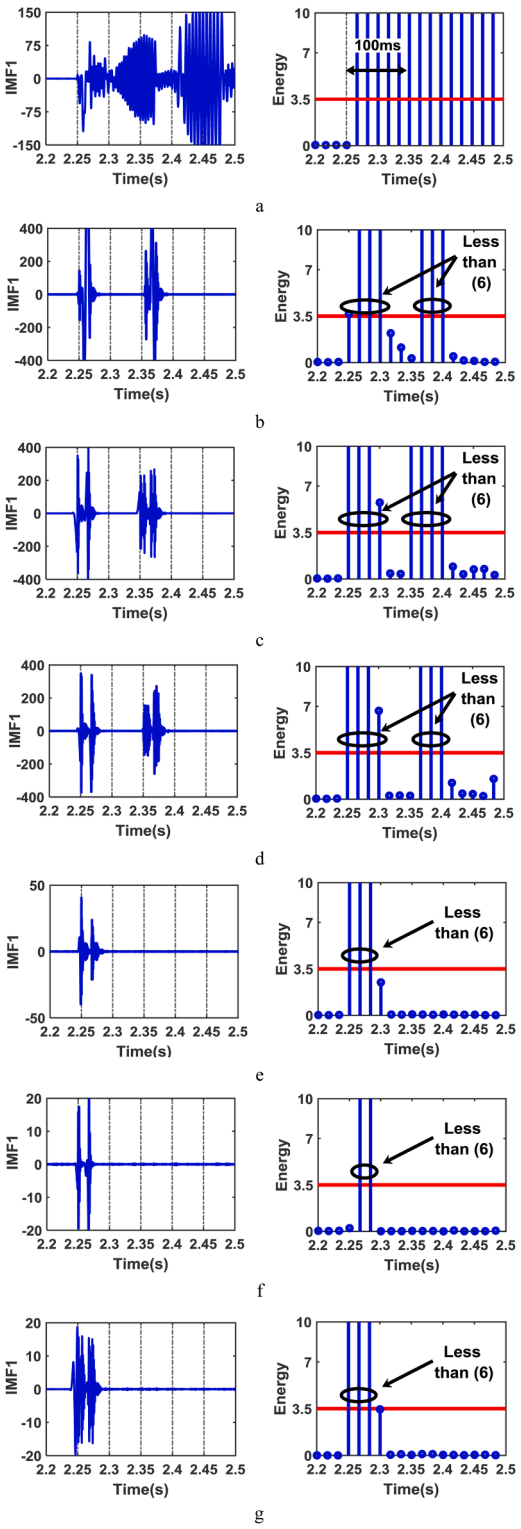

Fig. 28. Performance evaluation of the proposed method for case 20 (0% nonlinear loads), (a) islanding, (b) LG with Rf = 1Ω, (c) LLG with Rf = 1Ω, (d) LLLG with Rf = 1Ω, (e) capacitor switching 1 MVAr, (f) closing 1 MVAr inductive load, (g) opening 1 MVAr inductive load.

that ROCOF correctly operates only for 3, 2 and 2 cases corresponding to the ROCOF setting 0.5, 0.8 and 1.1 respectively. However, the proposed method correctly identifies all 7 islanding cases.

Also, Fig. 20b, indicates that the ROCOF algorithm can correctly identify 2, 3 and 4 cases corresponding to the ROCOF setting 0.5, 0.8 and

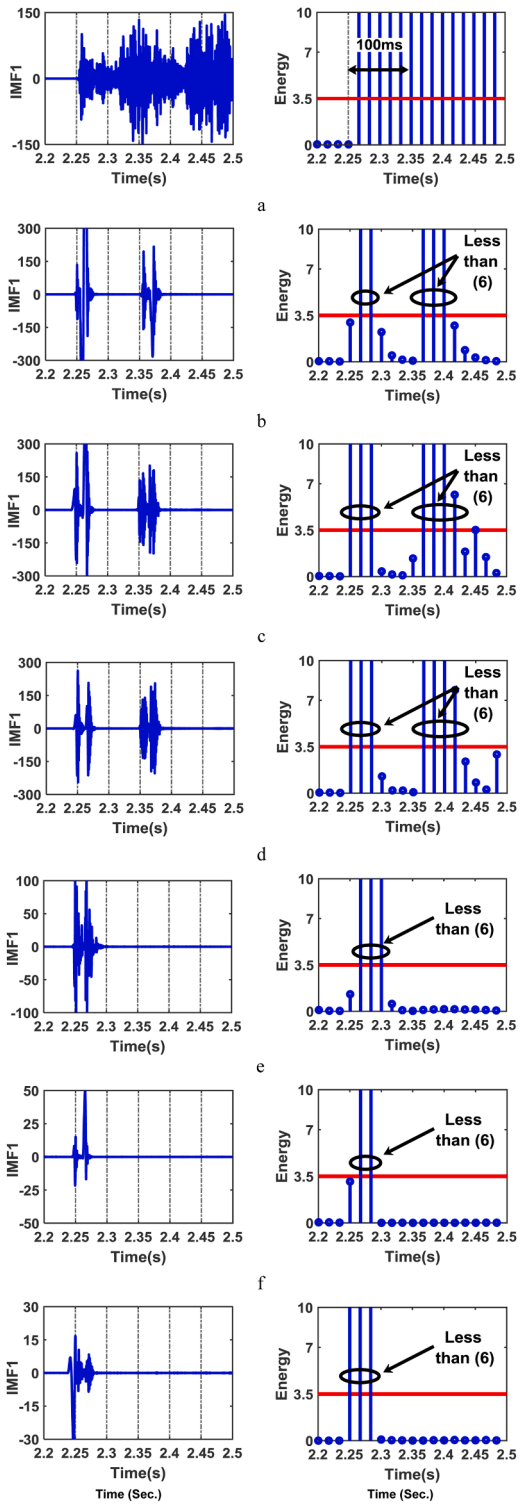

Fig. 29. Performance evaluation of the proposed method for case 21 (20% nonlinear loads), (a) islanding, (b) LG with Rf = 1Ω, (c) LLG with Rf = 1Ω, (d) LLLG with Rf = 1Ω, (e) capacitor switching 1 MVAr, (f) closing 1 MVAr inductive load, (g) opening 1 MVAr inductive load.

1.1 respectively. However, the proposed method correctly discriminates between islanding and non-islanding conditions in all 8 cases.

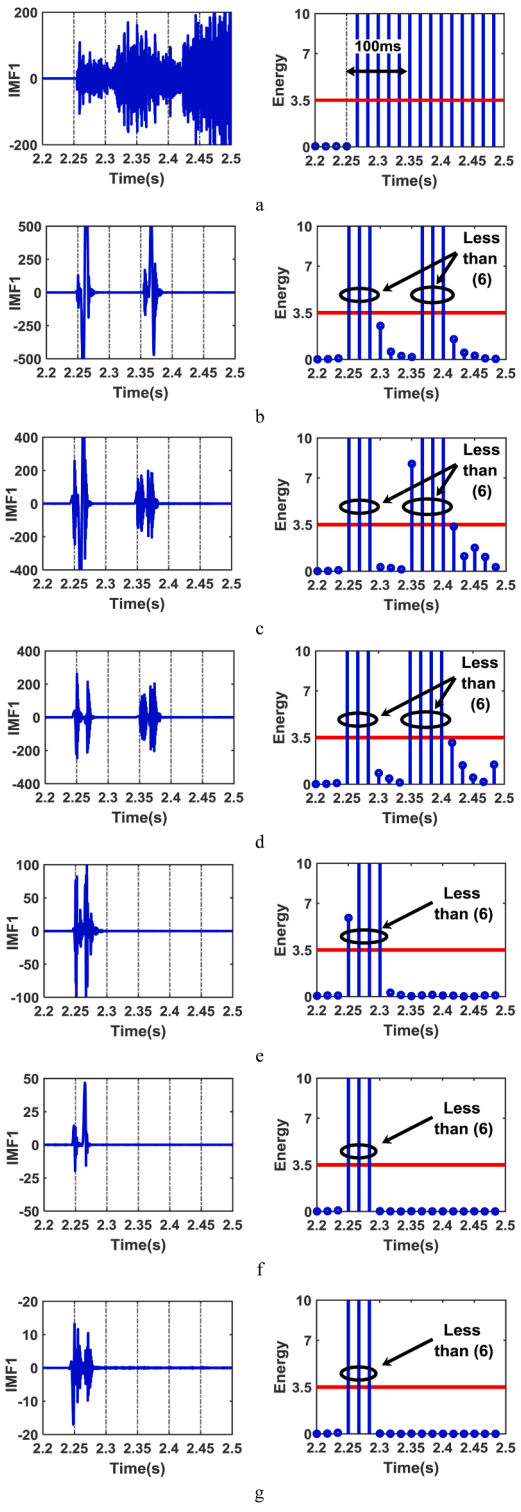

Fig. 30. Performance evaluation of the proposed method for case 22 (40% nonlinear loads), (a) islanding, (b) LG with Rf = 1Ω, (c) LLG with Rf = 1Ω, (d) LLLG with Rf = 1Ω, (e) Capacitor switching 1 MVAr, (f) Closing 1 MVAr Inductive load, (g) Opening 1 MVAr Inductive load.

3.8. Special cases

3.8.1. Performance evaluation for different types of loads i.e., constant power and constant current

Some cases are provided in Table 9 to evaluate the performance of the proposed algorithm for different types of loads. In this investigation,

Table 17
Maximum number of consecutive cycle of SE for different scenarios in the presence of harmonic loads.

Case number	Maximum number of consecutive cycle of SE larger than 3.5						
	Islanding	One Phase Fault	Two Phase Fault	Three Phase Fault	Capacitor Bank Switching	Closing Load	Opening Load
Case 20	14	4	4	4	3	2	3
Case 21	14	3	4	4	3	2	3
Case 22	14	4	4	4	4	3	3

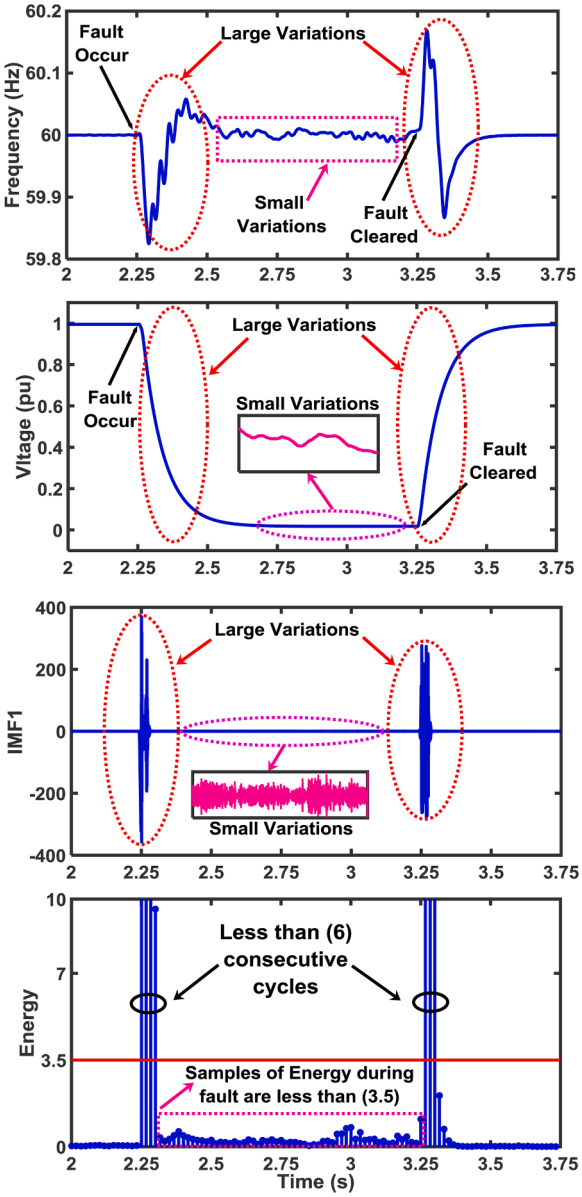

Fig. 31. Performance evaluation for three phase short circuit fault with R_f=0.05 Ω.

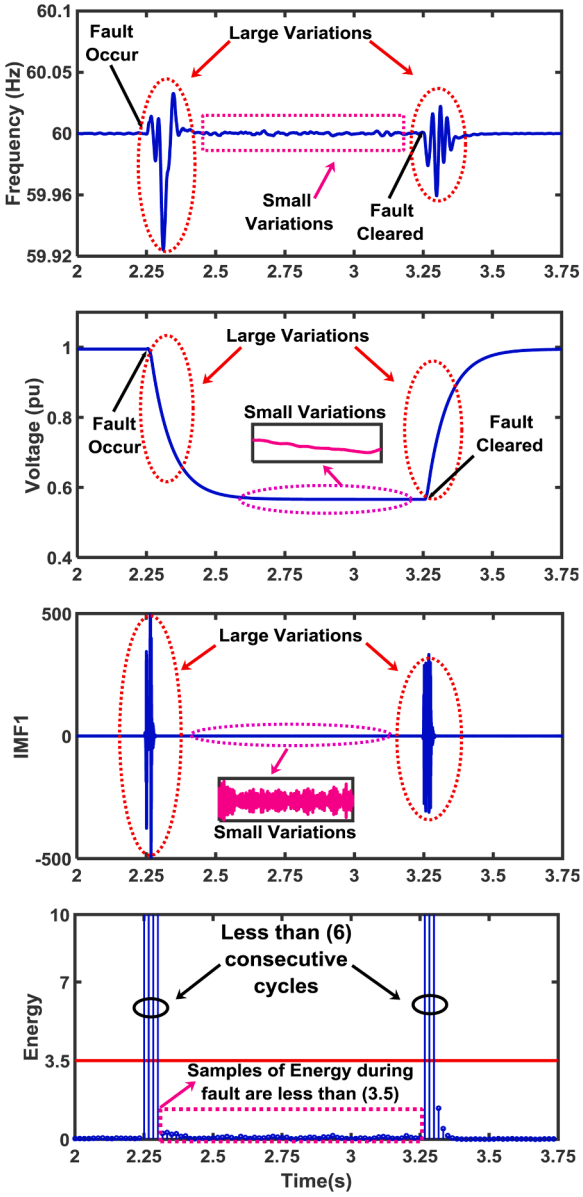

Fig. 32. Performance evaluation for two phase short circuit fault with R_f=0.05 Ω.

it has been assumed that while the active power has some level of unbalance, the reactive power of the load has full balance which result in difficult situation in islanding detection. After breaker opening at t = 2.25 s, the microgrid becomes islanded and as it can be seen in Figs. 21–24, the proposed index shows islanding is detected since it takes values more than threshold for at least 6 consecutive cycles of energy.

Also, several numerical results are provided in Table 10. This table shows the maximum number of consecutive cycle of SE which has value larger than threshold (i.e., 3.5) from t = 2.25 s to t = 2.5 s. According to Table 10, the proposed method can identify islanding condition for different load types.

3.8.2. *Performance evaluation for IEEE 34-bus distribution system*

In order to verify the accountability of the proposed approach, the IEEE 34 bus radial distribution grid has been adopted as the testbed. The selected distribution network is an unbalance network which contains several different types of loads [52]. According to Fig. 25, four areas are specified in the single line diagram of IEEE 34 bus network. The specifications of each area is tabulated in Table 11. Note that DG1 to DG4 are installed at buses 840, 860, 890 and 854. The specifications of each DGs

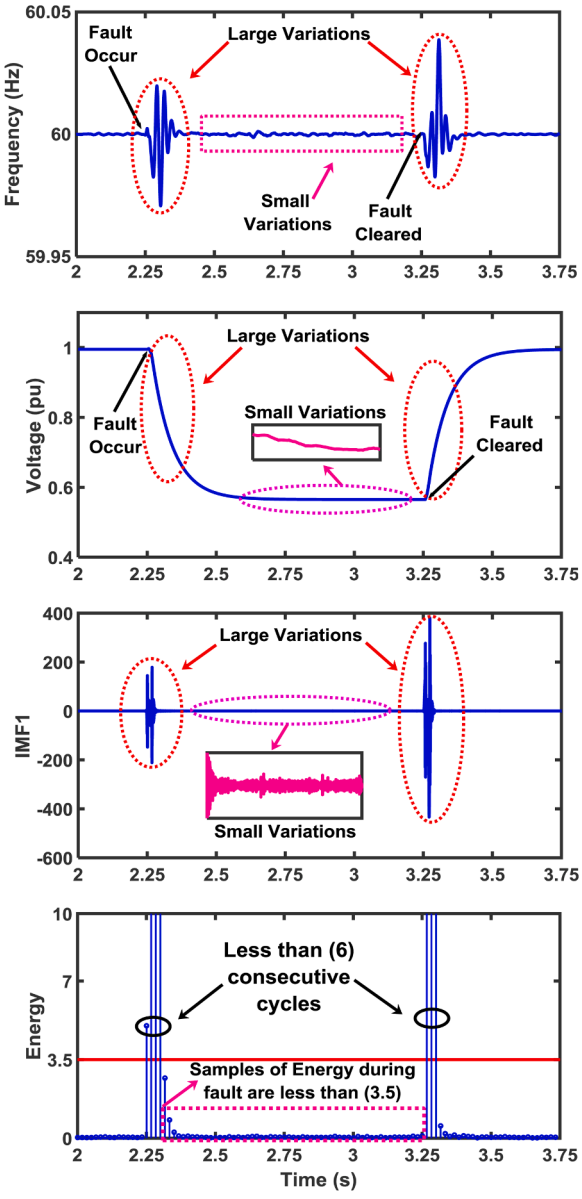

Fig. 33. Performance evaluation for one phase short circuit fault with R_f= 0.05 Ω.

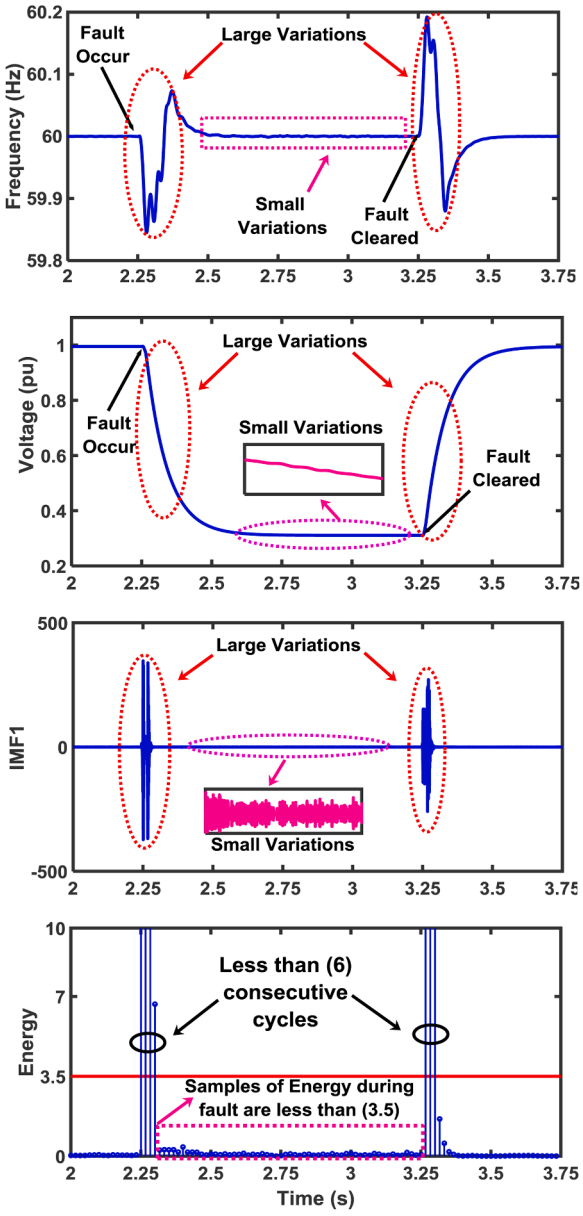

Fig. 34. Performance evaluation for one phase short circuit fault with R_f=1 Ω.

is provided in appendix. Several islanding and non-islanding scenarios are investigated in IEEE 34 bus network.

By opening CB 4 at t = 2.25 s, four DGs in area 4 become islanded. As shown in Fig. 26, the proposed index for all DGs has correctly identified islanding condition.

To investigate the performance of the proposed islanding detection method under fault condition, a three-phase fault with 0.1 s duration is applied at bus 858. As shown in Fig. 27, the proposed index does not remain above the threshold for more than 6 consecutive cycles. As a result, the proposed algorithm, does not mal-operate during fault condition.

In addition to the illustrative results, several numerical results with/without network reconfiguration for islanding and non-islanding scenarios are provided in Tables 12–15. According to the latter mentioned tables, the maximum number of consecutive cycle of SE has value larger than threshold (i.e., 3.5) from t = 2.25 s to t = 2.5 s. Note that in the case of network reconfiguration, the sectionalizing switch between buses 852 and 854 is opened and the tie switch between buses 816 and 852 is closed. Also feeder 1 and feeder 2 in Tables 14 and 15 located between

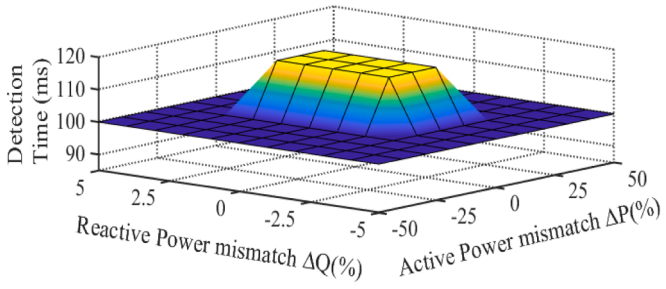

Fig. 35. Detection time of the proposed scheme for various power mismatches.

buses 858 and 840 and buses 858 and 854. The results indicate the proposed method is able to deal with different islanding and non-islanding conditions.

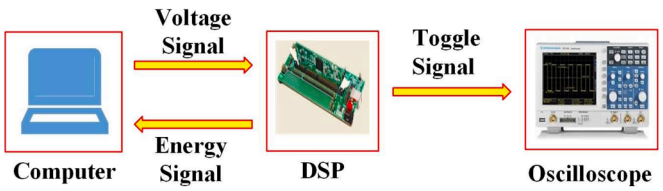

Fig. 36. The schematic of the employed test bench.

Table 18
Islanding condition for real time validation.

Case number	△P	△Q	Test system
Case 23	5%	0	2-bus test system shown in Fig. 2
Case 24	15%	1%	2-bus test system shown in Fig. 2

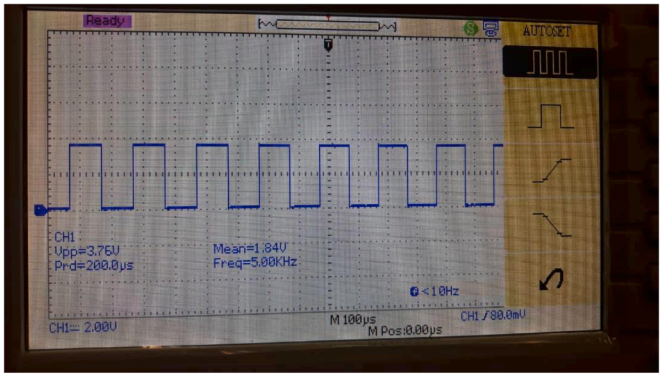

Fig. 37. Toggle signal of the proposed method.

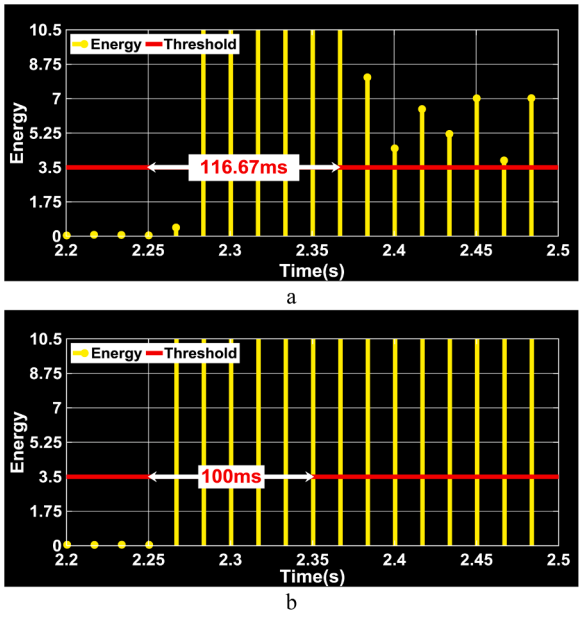

Fig. 38. Real-time validation of the proposed scheme, (a) Energy signal for case 23, (b) Energy signal for case 24.

3.8.3. *Performance evaluation in presence of harmonic in the network*

To show the effectiveness of the proposed method considering harmonics in the network, three cases are provided in Table 16. These cases are applied on IEEE 34 bus test system. According to Table 16, a percent of total linear loads is substituted with nonlinear loads. The nonlinear load is modelled with three-phase diode-rectifier load since the current rectifiers draw is not linear and generates harmonics. Note that in all islanding cases, by opening CB1 in area1, DG1 become islanded.

Several islanding and non-islanding scenarios are shown in Figs. 28–30.

As it can be observed from Table 17, even in the presence of harmonic loads, the proposed method can identify islanding scenarios. Also in the case of non-islanding conditions, the proposed method has robustness against various conditions and the threshold is not violated.

3.8.4. *Performance evaluation for long long-duration fault conditions*

Performance evaluation of the proposed method has been evaluated under some long-duration fault conditions. The results are shown in Figs. 31–34. As one can see in these figures, it is concluded that even in the case of 1s fault duration, the proposed index can robustly operate without malfunctioning. As discussed in the paper, according to Eq. (13), the proposed index basically depends on the voltage and frequency variations. While according to Figs. 31–34, during fault occurrence and clearance, the variations of the voltage and frequency is significant, in most of the time, the variations of voltage and frequency are small. Overall, in all cases, the proposed index does not violate the decision criterion for more than 6 cycles of SE and no islanding condition is detected.

4. Islanding detection time, hardware validation and NDZ of proposed method

4.1. *Response time*

Fig. 35 illustrates the delay response of the proposed algorithm for different levels of unbalance between load and generation. As one can see in Fig. 35, the proposed method has time delay between 100 to 116.67 ms. According to IEEE1547 [53], the islanding detection time delay is 2 second which indicate the proposed method has notable time response.

4.2. *Execution time*

The computation burden and operation time can be calculated in MATLAB using "Tick Count" and "tic-toc" respectively. The calculation's procedure of the proposed method is as follow:

- Calculating Δv for each phase. $(\Delta v(t) = v(t) - v(t - \Delta t))$
- Phasor estimation of $\Delta v(t)$.
- Calculating *PSVSV*. Note that *PSVSV* is the magnitude of positive sequence of $\Delta v(t)$.
- Calculating the *IPSVSV*.
- Calculating the signal energy of *IPSVSV* (i.e., SE signal).

The required time for above calculations, using a computer with core i5-5200U up to 2.7 GHz and 4 GB memory in MATLAB is about 5.36 µs which is much lower than step time (i.e. 100 µs). Therefore, the proposed method can be applied for real-time application.

4.3. *Hardware validation of proposed method*

Real time validation of the proposed scheme is carried out using DSP processor. To this end, a processor called TMDSCNCD28335 board, which has similar performance compared with the employed processors in protection relays is utilized. Accuracy and speed of the implemented algorithm in practice are the main criteria for judging the performance of the method in practice. A schematic of the employed test bench for evaluation of the method in the real application is shown in Fig. 36. The test bench includes a computer with Ci5-5200U CPU, a TMDSCNCD28335 board, and an oscilloscope to record the toggle signal. The processor has high-performance static CMOS technology – up

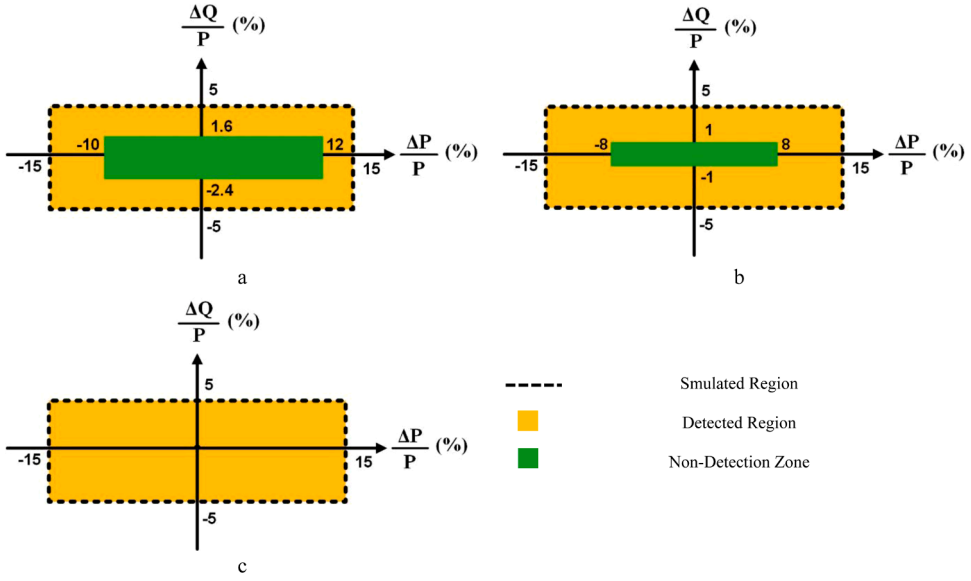

Fig. 39. NDZ region, (a) NDZ of voltage and frequency relays, (b) NDZ of ROCOF relay, (c) NDZ of proposed method.

Table 19
Comparative assessment of the proposed scheme with the techniques based on EMD.

Method	NDZ	LQF	Fault	CS	SIM	NLL	DG Type	AI (%)	ANI (%)	Limitation
Ref.[30]	5 %	-	-	√	-	√	SG	68.96	84.75	It requires both current and voltage signals, which increases the overall implementation cost
Ref.[31]	0 %	√	-	-	-	-	PV	100	81/92	It issues nuisance tripping during critical non-Islanding events
Ref.[32]	0 %	-	-	√	√	-	SG&WT	94/83	90.97	It is very difficult to decide multiple thresholds. It require further frequency estimation processes.
Ref.[33]	0 %	√	√	√	-	√	PV	98/27	95/49	It requires both current and voltage signals, which increases the overall implementation cost. Difficulty in selecting K value, dependency on initial values.
Proposed Method	0 %	√	√	√	√	√	PV&SG &WT	100	99.7	-

'√' and '–' indicates operating condition verified and not considered, respectively. CS: Capacitor Switching, SIM: Switching Induction Motor, NLL: Non-Linear Load switching, SG: Synchronous Generator, WT: Wind Turbine, AI: Accuracy for Islanding, ANI: Accuracy for Non-Islanding

Table 20
Types and number of test cases.

Event	Parameter	Variation in parameter	Cases Generated
Islanding	Active power mismatch	-50% to -5% in step of 5%	10
		-4% to 4% in step of 1%	9
		5% to 50% in step of 5%	10
	Reactive power mismatch	-50% to -5% in step of 5%	10
		-4% to 4% in step of 1%	9
		5% to 50% in step of 5%	10
Total islanding cases generated			58
Non-Islanding	Fault	Types of fault: LG, LL, LLG, LLL and LLLG. Total = 5 Fault Resistance (R_f): 0.01, 1, 5, 10 and 20 Ω. Total = 5 Fault Location: 20%, 40%, 60%, 80% and 90% of feeder between buses 832-890 and 858-860. Total = 10	5 × 5 × 10 = 250
	Switching of Capacitor bank	(i) Connecting: changing in rating of capacitor from 5μF to 100μF in steps of 10μF. Total = 20 (ii) Disconnecting: changing in rating of capacitor from 5μF to 100μF in steps of 10μF. Total = 20	20+20 = 40
	Starting Induction Motor load switching	Motor rating: 1hp, 10hp, 100hp, 1000hp. Total = 4	4
		(i) Connecting: changing in rating of load from 0.1 MVA to 1.5 MVA in steps of 0.1 MVA with PF. = 0.8 (lead/lag). Total = 30 (ii) Disconnecting: changing in rating of capacitor from 0.1 MVA to 1.5 MVA in steps of 0.1 MVA with PF. = 0.8 (lead/lag). Total = 30	30+30 = 60
Total non-islanding cases generated			354

to 150 MHz (6.67 ns Cycle Time). In addition, it includes 256K × 16 flash memory and 34K × 16 SARAM memory on the chip. During DSP implementation, the islanding conditions in Table 18 are considered. The voltage signal is sent through a serial communication link from PC to DSP with a sampling frequency of 10 kHz. The DSP processes the received data and sends the energy signal to the computer. The toggle signal confirms that the processor can handle the calculations in real-time. Fig. 37 shows the toggle signal steps in each sampling period.

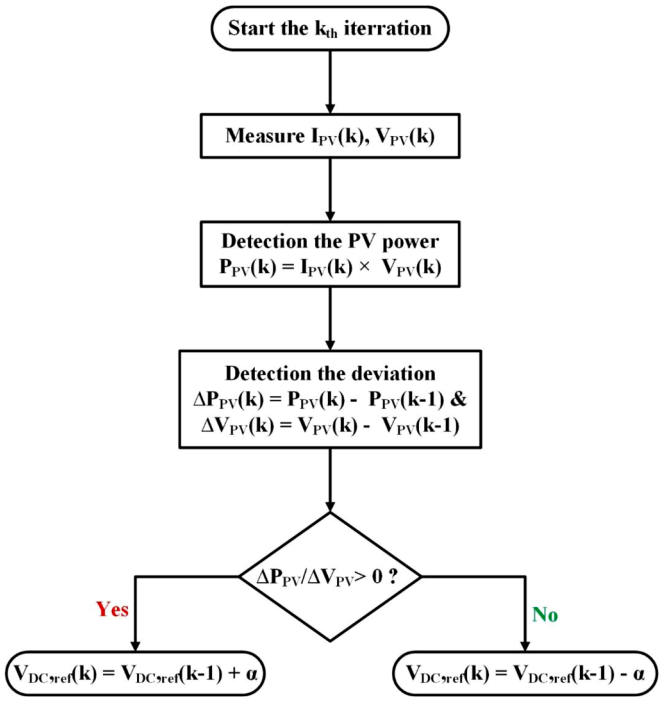

Fig. 40. Flowchart of 'Perturb and Observe' (P&O) MPPT method.

From Fig. 38, it can be seen that the proposed index identifies the islanding condition.

4.4. NDZ of proposed method

Thanks for the comment. Several cases are conducted in Sections 3.2–3.4 (please see Figs. 5 and 7–11) that show the performance of the proposed method under zero and small power imbalance. According to these cases, even in the very small power imbalance, the variation in the IPSVSV are significant and the proposed index can robustly detect islanding condition. However, to effectively show the proposed method performance in the case of small power imbalance, the NDZ for proposed method, voltage and frequency relays and ROCOF method with setting 0.5 Hz/s is provided in Fig. 39. To obtain Fig. 39, large number of islanding cases were simulated with different values of active and reactive power unbalance (from −15 % to 15% of active power mismatch with step of 0.2% and -5% to 5% of reactive power mismatch with step of 0.1%). The NDZ of each method (green region) with the total area of simulated power unbalance (area shown by dashed line) are presented in Fig. 39. As shown in Fig. 39 and as well as in Sections 3.2–3.4 (please see Figs. 5 and 7–11), while voltage and frequency relays and ROCOF methods have notable NDZ regions in comparison with the proposed method. Due to small power imbalance, the voltage, frequency and ROCOF are changed slightly. As a result, voltage and frequency relays and ROCOF methods may experience mal-operation during small power imbalance. However, even in the case of slight voltage and frequency changes during small power imbalance, the proposed islanding detection changes significantly so that the islanding condition can be precisely detected.

5. Comparison with state-of-the-art algorithms

Table 19 summarizes the specifications and limitations of some of the EMD based islanding detection techniques [30–33].

Utilizing several islanding and non-islanding scenarios given in Table 20, the performance of the proposed scheme is compared with the methods reported in [30–33]. Note that due to inability [30–33] to deal with some type of DGs, each method only evaluated for the mentioned types of DG in Table 19. Also, the comparison is carried out on IEEE 34 bus distribution test system.

After simulation of all these cases, performance of these islanding detection techniques is analysed for critical islanding and non-islanding events. The true detection rates for all scenarios are calculated and provided in Table 19. From Table 19, it is observed that the method in [30] detects 68.96% of islanding scenarios accurately, whereas it experiences maloperation for 15.25% of non-islanding (i.e. fault and starting induction motor events). Further, it is noted that [31] detects critical islanding scenarios, however, it only detects 81.92% of non-islanding cases. Moreover, the method in [32] can detect 94.83% of islanding scenarios accurately, whereas it has 90.97% accuracy for non-islanding cases. Finally, the method in [33] detects 98.27% of islanding scenarios, whereas it has 95.49% accuracy for non-islanding cases. As it can be observed in Table 19, the proposed islanding detection technique provides the highest islanding detection rate and simultaneously the highest rate of robustness in correct discrimination between islanding events and non-islanding events.

6. Conclusion

In this paper, an islanding detection algorithm was developed. The proposed algorithm utilizes voltage signal measured at the PCC point, to obtain the PSVSV. Proposed algorithm was designed to employ EMD to

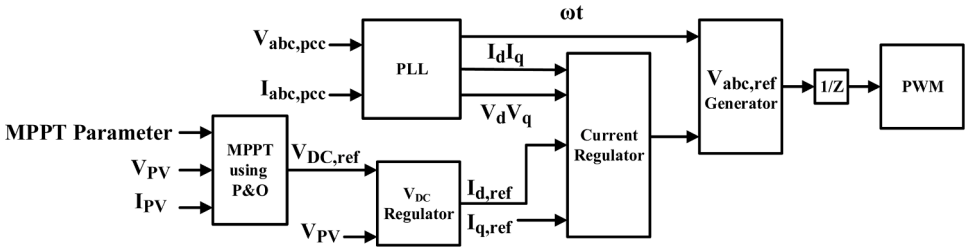

Fig. 41. Block diagram of constant current inverter.

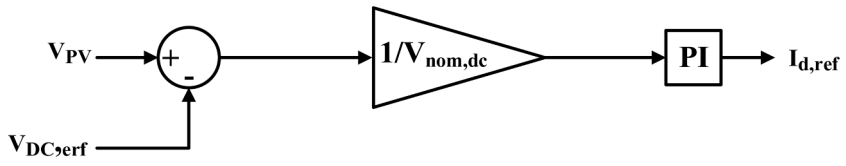

Fig. 42. Block diagram of DC voltage regulator.

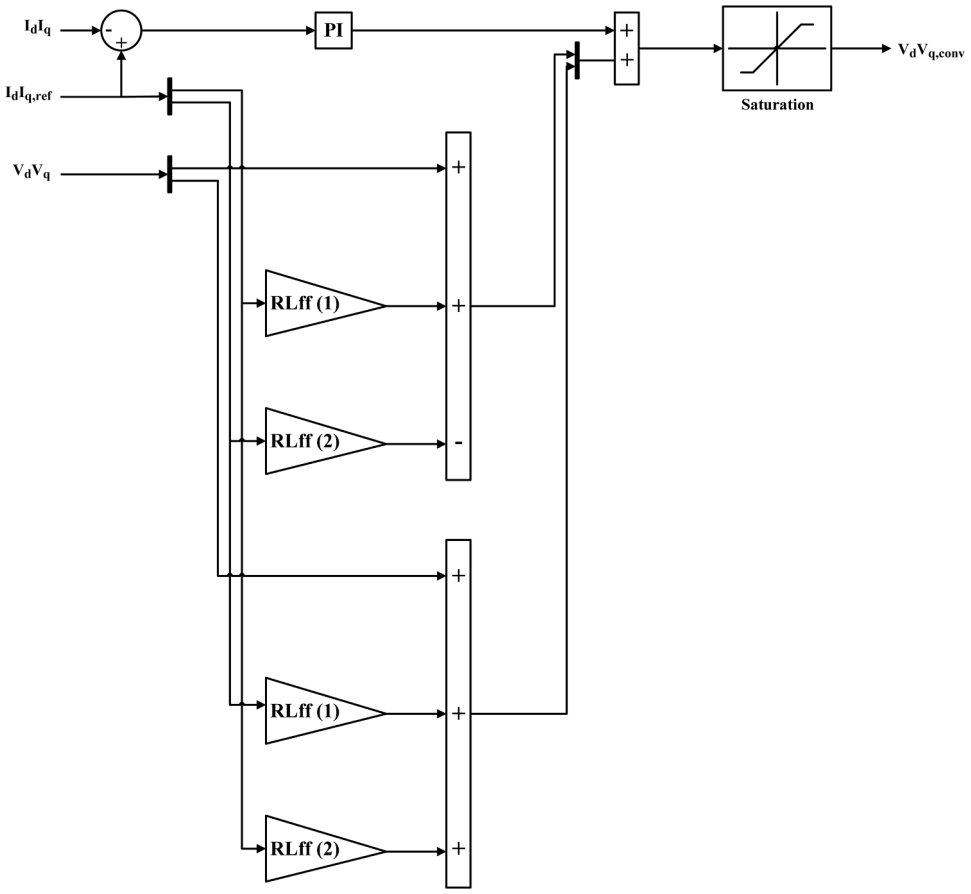

Fig. 43. Block diagram of current regulator.

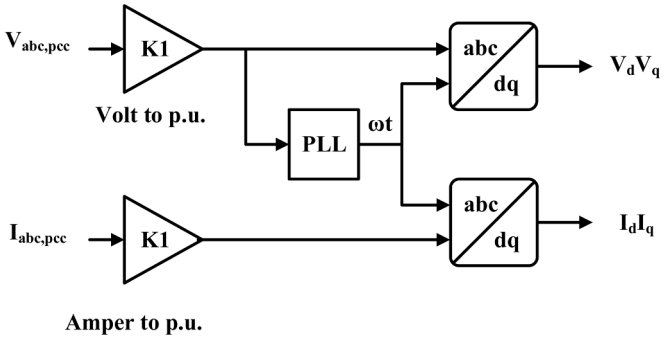

Fig. 44. Block diagram of PLL and measurement regulator.

extract first intrinsic mode functions (IMF) of PSVSV. Eventually, a new index for islanding detection was proposed for the signal energy of first IMF of PSVSV. As demonstrated, the proposed index can clearly discriminate for islanded and non-islanded conditions after a short time interval. Simulation results indicate that the proposed index can comprehensively deal with different circumstances and discriminate between islanding and non-islanding conditions. Comparing with the previous published passive algorithms, the proposed method has zero NDZ and it can identify islanding condition when the system has full balance between load and generation. Unlike active method, the proposed method has not inappropriate effects on the power quality issues of microgrids. In addition of comprehensiveness, the proposed algorithm has straightforward implementation, high accuracy, and notable speed of islanding detection. As a result, the proposed algorithm can be implemented for islanding detection in the microgrids.

Table 21
Parameters of MPPT, DC voltage and current regulator.

Parameter	Value
MPPT	
Initial value for $V_{DC,ref}$	480 V
Maximum value for $V_{DC,ref}$	375 V
Minimum value for $V_{DC,ref}$	583 V
Increment value used to increase/decrease $V_{DC,ref}$ (α)	0.01
DC Voltage Regulator	
K_p	2
K_i	400
$V_{nom,dc}$	480 V
Current Regulator	
K_p	0.3
K_i	20
RLff (1)	0.0039
RLff (2)	0.21
Lower limit of saturation	-1.5
Upper limit of saturation	1.5

CRediT authorship contribution statement

Hasan Khosravi: Data curation, Formal analysis, Methodology, Validation, Visualization, Software, Writing – original draft, Writing – review & editing. **Haidar Samet:** Resources, Investigation, Methodology, Funding acquisition, Project administration, Supervision, Writing – review & editing. **Mohsen Tajdinian:** Formal analysis, Investigation, Methodology, Writing – original draft, Writing – review & editing.

Declaration of Competing Interest

The authors declare that they have no known competing financial

Table 22
Specifications of DGs utilized in IEEE 34-bus network.

Parameter	Value
Solar panel power parameter (DG1 & DG2)	
Rated capacity	2.5 MVA
Number of series connected cell per string per PV module	36
Number of parallel string of cells per PV module	1
Number of PV module in series	115
Number of PV module in parallel	285
285 pen circuit Voltage per PV module	21.7 V
Short circuit current per PV module	3.35 A
Reference temperature	25°C
Reference solar intensity	1000W/ m2
Synchronous generators parameters (DG3)	
Rated capacity	1MVA
Rated RMS line-to-neutral voltage	2.4KV base
angular frequency: 50Hz Inertia constant (H)	1.71
MWs/KVA Stator resistance (Ra)	0.003pu
Stator leakage reactance (Xa)	0.088pu
Direct-axis unsaturated reactance (Xd)	1.56pu
Direct-axis unsaturated transient reactance (Xd′)	0.26pu
Direct-axis unsaturated sub-transient reactance (Xd′)	0.15pu
Quadrature-axis unsaturated reactance (Xq)	1.06pu
Quadrature-axis unsaturated transient reactance (Xq′)	0.62pu
Quadrature-axis unsaturated sub-transient reactance (Xq′)	0.15pu
Direct-axis unsaturated transient open time constant (Td0′)	3.7s
Direct-axis unsaturated sub-transient open time constant (Td0′)	0.05s
Quadrature-axis unsaturated transient open time constant (Tq0′)	0.3s
Quadrature-axis unsaturated sub-transient open time constant (Tq0′)	0.05s
Exciter parameters of Synchronous generators (IEEE type ST1 excitation system)	
Voltage regulator time constant (Ta)	0.02s
Voltage regulator gain (Ka)	200
AVR lag time constant (Tb)	20.0s
AVR lead time constant (Tc)	1.0s
Excitation system regulation factor (Kc)	0.175
Maximum controller output (Vrmx)	5.7pu
Minimum controller output (Vrmn)	−4.9pu
Wind Turbine parameter (DG4)	
Rated capacity	0.5 MVA
Voltage	690 V base
Stator resistance Rs	0.0078 pu.
Rotor resistance Rr	0.0078 pu.
Stator leakage inductance Xss	0.0794 pu.
Rotor leakage inductance Xrs	0.1158 pu.
Mutual inductance Xm	4.104 pu.
Per unit inertia constant of generator Hg	0.52 s
Transformation reactance Xtr	0.025 pu.
A single transmission line reactance Xl	0.0013 pu.

interests or personal relationships that could have appeared to influence the work reported in this paper.

Appendix

The flowchart of the employed MPPT is given in Fig. 40. The fundamental principle of the 'Perturb and Observe' (P&O) method is designed based on the purposely perturbing the voltage, and then comparing the power to the acquired before to disruption. Extremely, if the power is raised due to disruption, the new perturbation will be made in the same direction. Otherwise if the power fall, the new perturbation is made in the opposite direction. The P&O always holds the following condition:

$$\frac{\partial P_{PV}}{\partial V_{PV}} = 0 \tag{17}$$

where P_{PV}, and V_{PV} are the PV module output power and voltage, respectively. Through the implementation procedure, the output current and voltage of the PV module are periodically observed at sequential sampling steps in order to determine the corresponding output power and power derivation with voltage. The block diagrams of the constant current controlled inverter and its major subsystems *are* given in Figs. 41–44. The descriptions of these block diagrams are provided in Section 3. The parameters of the constant current controlled inverter and its major subsystems are given in Table 21. The specifications of each DGs utilized in IEEE 34-bus network are shown in Table 22.

References

[1] C.L. Trujillo, D. Velasco, E. Figueres, G. Garcerá, Analysis of active islanding detection methods for grid-connected microinverters for renewable energy processing, Appl. Energy 87 (11) (2010) 3591–3605.

[2] F. Hashemi, N. Ghadimi, B. Sobhani, Islanding detection for inverter-based DG coupled with using an adaptive neuro-fuzzy inference system, Int. J. Electr. Power Energy Syst. 45 (1) (2013) 443–455.

[3] Standards Coordinating Committee 21 on Fuel Cells, Photovoltaic, Dispersed Generation, and Energy Storage: 'IEEE Standard for Interconnecting Distributed Resources with Electric Power Systems', (IEEE-Std1547T M-2003 IEEE, Inc, USA, 2003, pp. 1–15, 3 Park Avenue, NY10016-5997July.

[4] A.M. Massoud, K.H. Ahmed, S.J. Finney, B.W. Williams, Harmonic distortion-based island detection technique for inverter-based distributed generation, IET Renew. Power Gener. 3 (4) (2009) 493–507.

[5] M.A. Redfern, O. Usta, G. Fielding, Protection against loss of utility grid supply for a dispersed storage and generation unit, IEEE Trans. Power Deliv. 8 (3) (1993) 948–954.

[6] M.E. Ropp, K. Aaker, J. Haigh, N. Sabbah, Using power line carrier communications to prevent islanding [of PV power systems].", in: Conference Record of the Twenty-Eighth IEEE Photovoltaic Specialists Conference-2000, IEEE, 2000, pp. 1675–1678 (Cat. No. 00CH37036).

[7] W. Xu, G. Zhang, C. Li, W. Wang, G. Wang, J. Kliber, A power line signaling based technique for anti-islanding protection of distributed generators—part I: scheme and analysis, IEEE Trans. Power Deliv. 22 (3) (2007) 1758–1766.

[8] H. Samet, F. Hashemi, T. Ghanbari, Minimum non detection zone for islanding detection using an optimal artificial neural network algorithm based on PSO, Renew. Sustain. Energy Rev. 52 (2015) 1–18.

[9] K. Sareen, B.R. Bhalja, R.P. Maheshwari, Universal islanding detection technique based on rate of change of sequence components of currents for distributed generations, IET Renew. Power Gener. 10 (2) (2016) 228–237.

[10] K. Sareen, B.R. Bhalja, R.P. Maheshwari, Islanding detection technique based on inverse hyperbolic secant function, IET Renew. Power Gener. 10 (7) (2016) 1002–1009.

[11] H. Samet, F. Hashemi, T. Ghanbari, Islanding detection method for inverter-based distributed generation with negligible non-detection zone using energy of rate of change of voltage phase angle, IET Gener. Transm. Distrib. 9 (15) (2015) 2337–2350.

[12] P. Gupta, R.S. Bhatia, D.K. Jain, Active ROCOF relay for islanding detection, IEEE Trans. Power Deliv. 32 (1) (2016) 420–429.

[13] D. Voglitsis, F. Valsamas, N. Rigogiannis, N. Papanikolaou, On the injection of sub/inter-harmonic current components for active anti-islanding purposes.", Energies 11 (9) (2018) 2183.

[14] D. Voglitsis, N. Papanikolaou, ACh Kyritsis, Incorporation of harmonic injection in an interleaved flyback inverter for the implementation of an active anti-islanding technique, IEEE Trans. Power Electron. 32 (11) (2016) 8526–8543.

[15] A. Emadi, H. Afrakhte, A reference current perturbation method for islanding detection of a multi-inverter system, Electric Power Syst. Res. 132 (2016) 47–55.

[16] R. Zamani, M.-E. Hamedani-Golshan, H.H. Alhelou, P. Siano, H.R. Pota, Islanding detection of synchronous distributed generator based on the active and reactive power control loops, Energies 11 (10) (2018) 2819.

[17] N.A. Fadzil, M.H. Hairi, F. Hanaffi, M.N. Kamarudin, A.S. Isira, M.F.P. Mohamed, N. Amirah Fadzil, A research of islanding detection method for distributed generation: mechanism, merits and demerits, Int. J. Innov. Technol. Explor. Eng. (IJITEE) 8 (12S2) (October 2019) 508–520. ISSN: 2278-3075.

[18] M. Khodaparastan, H. Vahedi, F. Khazaeli, H. Oraee, A novel hybrid islanding detection method for inverter-based DGs using SFS and ROCOF, IEEE Trans. Power Deliv. 32 (5) (2015) 2162–2170.

[19] C.-T. Hsieh, J.-M. Lin, S.-J. Huang, Enhancement of islanding-detection of distributed generation systems via wavelet transform-based approaches, Int. J. Electr. Power Energy Syst. 30 (10) (2008) 575–580.

[20] S.R. Samantaray, A. Samui, B.C. Babu, Time-frequency transform-based islanding detection in distributed generation, IET Renew. Power Gener. 5 (6) (2011) 431–438.

[21] M. Hanif, M. Basu, K. Gaughan, Development of EN50438 compliant wavelet-based islanding detection technique for three-phase static distributed generation systems, IET Renew. Power Gener. 6 (4) (2012) 289–301.

[22] P.K. Ray, N. Kishor, S.R. Mohanty, Islanding and power quality disturbance detection in grid-connected hybrid power system using wavelet and $ S $-transform, IEEE Trans. Smart Grid 3 (3) (2012) 1082–1094.

[23] P.K. Dash, M. Padhee, T.K. Panigrahi, A hybrid time–frequency approach based fuzzy logic system for power island detection in grid connected distributed generation, Int. J. Electr. Power Energy Syst. 42 (1) (2012) 453–464.

[24] A. Samui, S.R. Samantaray, Wavelet singular entropy-based islanding detection in distributed generation, IEEE Trans. Power Deliv. 28 (1) (2012) 411–418.

[25] N.E. Huang, Z. Shen, S.R. Long, M.C. Wu, H.H. Shih, Q. Zheng, N.-C. Yen, C. C. Tung, H.H. Liu, The empirical mode decomposition and the Hilbert spectrum for nonlinear and non-stationary time series analysis, Proc. R. Soc. Lond. Ser. A 454 (1971) (1998) 903–995.

[26] N.E.h. Huang, Hilbert-Huang Transform and its Applications, 16, World Scientific, 2014.

[27] N.E. Huang, M.-L. Wu, W. Qu, S.R. Long, S.S.P. Shen, Applications of Hilbert–Huang transform to non-stationary financial time series analysis, Appl. Stoch. Models Bus. Ind. 19 (3) (2003) 245–268.

[28] Z.K. Peng, W.T Peter, F.L. Chu, A comparison study of improved Hilbert–Huang transform and wavelet transform: application to fault diagnosis for rolling bearing, Mech. Syst. Sig. Process. 19 (5) (2005) 974–988.

[29] A.Y. Ayenu-Prah, N.O. Attoh-Okine, Comparative study of Hilbert–Huang transform, Fourier transform and wavelet transform in pavement profile analysis, Veh. Syst. Dyn. 47 (4) (2009) 437–456.

[30] B.K. Chaitanya, A. Yadav, Hilbert–huang transform based islanding detection scheme for distributed generation, in: 2018 IEEE 8th Power India International Conference (PIICON), IEEE, 2018, pp. 1–5.

[31] A.H.M. Niaki, S. Afsharnia, A new passive islanding detection method and its performance evaluation for multi-DG systems, Electr. Power Syst. Res. 110 (2014) 180–187.

[32] A. Doroozi, J. Olamaei, A new passive islanding detection method for distributed generations using time-frequency transform-based EMD-HT, Signal Process. Renew. Energy 1 (4) (2017) 9–25.

[33] S.R. Thomas, V. Kurupath, U. Nair, A passive islanding detection method based on K-means clustering and EMD of reactive power signal, Sustain. Energy Grids Netw. 23 (2020), 100377.

[34] R. Dubey, M. Popov, S.R. Samantaray, Transient monitoring function-based islanding detection in power distribution network, IET Gener. Transm. Distrib. 13 (6) (2018) 805–813.

[35] R. Nale, M. Biswal, N. Kishor, A transient component based approach for islanding detection in distributed generation, IEEE Trans. Sustain. Energy 10 (3) (2018) 1129–1138.

[36] M.A. Farhan, K. Shanti Swarup, Mathematical morphology-based islanding detection for distributed generation, IET Gener. Transm. Distrib. 10 (2) (2016) 518–525.

[37] S. Agrawal, S. Patra, S.R. Mohanty, V. Agarwal, M. Basu, Use of matrix-pencil method for efficient islanding detection in static DG and a parallel comparison with DWT method, IEEE Trans. Indust. Electron. 66 (11) (2018) 8937–8946.

[38] S. Admasie, S. Basit, A. Bukhari, R. Haider, T. Gush, C.-.H. Kim, A passive islanding detection scheme using variational mode decomposition-based mode singular entropy for integrated microgrids, Electr. Power Syst. Res. 177 (2019), 105983.

[39] H.S. Rupal, K.T. Ankit, S.R. Mohanty, N. Kishor, Detection and classification of power quality disturbances using signal processing techniques, in: Proc. IEEE PES Asia-Pacific Power Energy Eng. Conf., 2017, pp. 1–6.

[40] S. Biswal, M. Biswal, O.P. Malik, Hilbert huang transform based online differential relay algorithm for a shunt-compensated transmission line, IEEE Trans. Power Deliv. 33 (6) (2018) 2803–2811.

[41] M.K. Jena, B.K. Panigrahi, S.R. Samantaray, A new approach to power system disturbance assessment using wide-area postdisturbance records, IEEE Trans. Ind. Inf. 14 (3) (2017) 1253–1261.

[42] R. Sadeghi, H. Samet, T. Ghanbari, Detection of stator short-circuit faults in induction motors using the concept of instantaneous frequency, IEEE Trans. Ind. Inf. 15 (8) (2018) 4506–4515.

[43] Y. Kim, H. Jo, D. Kim, A new peak power tracker for cost-effective photovoltaic power system, in: IECEC 96. Proceedings of the 31st Intersociety Energy Conversion Engineering Conference 3, IEEE, 1996, pp. 1673–1678.

[44] Z.-K. Huang, K.-W. Chau, A new image thresholding method based on Gaussian mixture model, Appl. Math. Comput. 205 (2) (2008) 899–907.

[45] P. Moulin, J. Liu, Analysis of multi resolution image denoising schemes using generalized Gaussian and complexity priors, IEEE Trans. Inf. Theory 45 (3) (1999) 909–919.

[46] N. Otsu, A threshold selection method from gray-level histograms, Automatica 11 (285-296) (1975) 23–27.

[47] E. Cuevas, H. Sossa, A comparison of nature inspired algorithms for multi-threshold image segmentation, Expert Syst. Appl. 40 (4) (2013) 1213–1219.

[48] R. Guo, S.M. Pandit, Automatic threshold selection based on histogram modes and a discriminant criterion, Mach. Vis. Appl. 10 (5) (1998) 331–338.

[49] Static Inverter and Charge Controllers for Use in Photovoltaic Systems, (Underwriters Laboratories, Inc.,) Northbrook, IL, Standard UL, 2001.

[50] C.M. Affonso, W. Freitas, W. Xu, L.C.P. Da Silva, Performance of ROCOF relays for embedded generation applications, IEE Proc.-Gener. Transm. Distrib. 152 (1) (2005) 109–114.

[51] C.R Reddy, K. Harinadha Reddy, A new passive islanding detection technique for integrated distributed generation system using rate of change of regulator voltage over reactive power at balanced islanding, J. Electr. Engi. Technol. 14 (2) (2019) 527–534.

[52] Y.M. Makwana, B.R. Bhalja, Islanding detection technique based on superimposed components of voltage, IET Renew. Power Gener. 11 (11) (2017) 1371–1381.

[53] IEEE Standards Board, IEEE Standard for Interconnecting Distributed Resources with Electric Power Systems, IEEE, 2003, pp. 1547–2003.